S-PARAMETER MODELING OF TWO-PORT DEVICES USING A SINGLE, MEMORYLESS NONLINEARITY

by

Marc William Legori Ditz

Thesis submitted to the Faculty of the
Virginia Polytechnic Institute and State University
in partial fulfillment of the requirements for the degree of

MASTER OF SCIENCE

in

Electrical Engineering

APPROVED:

Donald M. Keller

Dr. D. M. Keller, Chair

William A. Davis

Dr. W. A. Davis

Sedki M. Riad

Dr. S. M. Riad

December, 1992

Blacksburg, Virginia

S-PARAMETER MODELING OF TWO-PORT DEVICES USING A SINGLE, MEMORYLESS NONLINEARITY

by

Marc William Legori Ditz

Committee Chair: Donald M. Keller

Electrical Engineering

(ABSTRACT)

It is proposed to represent a nonlinear two-port device by a scattering-parameter (S-parameter) model containing a single nonlinearity. Furthermore, it is proposed that the nonlinearity be modeled as a memoryless nonlinear function. A bipolar junction transistor (BJT) operating in the active region is suggested as one application of this modeling approach. The validity of the model is demonstrated by the comparison of measured and model-predicted data for a microwave BJT.

The proposed nonlinear model is represented by a linear three-port flow-graph having one of its ports terminated in a real-valued, nonlinear reflection. The model parameters are determined from measurements of device-under-test (DUT) transmission and reflection at various input drive levels. As an illustration of its utility, the model is applied to the design of an oscillator. The measured results of a constructed oscillator are provided.

A presentation of a new form of calibration for microwave measurement systems precedes the nonlinear modeling discussion. The new calibration technique combines the transmission line approach to calibration with a load-pull process common to nonlinear device measurements. A two-port, one-way measurement process obviates the need for DUT reversal. The calibrated measurement of input reflection, transmission, and load reflection is discussed. In addition, the procedure for determining the small-signal S parameters of the DUT is given.

To my grandmother Liliane Legori,
who has always encouraged me to go higher.

ACKNOWLEDGEMENTS

The author wishes to recognize the invaluable assistance of Drs. Donald M. Keller and William A. Davis, whose contributions to this work cannot be overemphasized. In a way, this is really their thesis as well.

Dr. Davis equipped the author with much of the conceptual foundation of this research in the form of extensive note-sets and personal communication. He could always willingly be called upon to answer questions, offer suggestions and technical assistance, and provide mechanical help in the preparation of this document.

Dr. Keller has shown a personal interest in this student's academic career at Virginia Tech. He has often gone beyond the call of duty, not only when providing expertise related to this thesis, but also when asked for general help with coursework and other educational concerns. Dr. Keller has been a superb teacher, both in the classroom and on an individual basis. The author feels fortunate to have been under his tutelage.

The author would also like to thank Raytheon Corporation for its generosity in helping fund this research. The willingness of Dr. Sedki Riad to serve as a committee member and to review the original manuscript is also appreciated.

Contents

CHAPTER 1: INTRODUCTION 1

1.1 Background 1

1.2 Previous Work 2

1.3 Proposed Techniques 5

1.4 Organization of Thesis 6

CHAPTER 2: CALIBRATION 7

2.1 Introduction 7

2.2 One-Port Models 8

2.3 Two-Port Models 10

2.4 Proposed One-Way Two-Port Model 13

2.4.1 Reflection 13

2.4.2 Isolation 19

2.4.3 Transmission 20

2.5 Device Measurements 21

2.6 S-Parameter Measurements 23

CHAPTER 3: NONLINEAR MODEL 25

3.1 Introduction 25

3.2 Model Representation 27

3.3 Determination of Model Parameters 29

3.3.1 Small-Signal 30

3.3.2 Choice of S_{33} 31

3.3.3 Finding S_{13}/S_{23} 37

3.3.4 Determining $S_{23}S_{31}$ and $S_{23}S_{32}$ 38
3.3.5 Solving for Individual Parameters 41
3.3.6 Characterizing Γ_N 42
3.4 Summary 43

CHAPTER 4: APPLICATIONS 44
4.1 Introduction 44
4.2 Prediction of Input Reflection and Transmission 45
4.3 Stability 50
4.4 Oscillator Design 52
4.4.1 Choosing Value for Γ_N 52
4.4.2 Oscillator Topology 53
4.4.3 Finding Source and Load Terminations 53
4.4.4 Output Level Prediction 57
4.4.5 Results 59

CHAPTER 5: CONCLUSION 62

REFERENCES 64

APPENDIX 66

VITA 68

List of Figures

Figure 2.1 One-port calibration model for microwave S-parameter measurements 9

Figure 2.2 Two-port calibration model for microwave S-parameter measurements 11

Figure 2.3 Proposed one-way two-port calibration model for microwave S-parameter measurements 14

Figure 3.1 Model for representation of two-port device having a single, memoryless nonlinearity 28

Figure 3.2 Circle fit to transmission data points. Input drive level limited to prevent saturation of device under test 32

Figure 3.3 Circle fit to reflection data points. Input drive level limited to prevent saturation of device under test 33

Figure 3.4 Circle fit to transmission data points. Input drive level becoming sufficiently high to saturate device under test 34

Figure 3.5 Circle fit to reflection data points. Input drive level becoming sufficiently high to saturate device under test 35

Figure 4.1 MRF901 BJT microwave amplifier characterization 46

Figure 4.2 Measured and predicted transmission versus input drive level for MRF901 BJT microwave amplifier 48

Figure 4.3 Measured and predicted reflection versus input drive level for MRF901 BJT microwave amplifier 49

Figure 4.4 (a) Generalized representation of an oscillator.
(b) Representation of oscillator topology chosen for design 54

Figure 4.5 Microstrip 880 MHz oscillator 60

Figure 4.6 Measured and predicted input reflection coefficient versus input drive level for MRF901 BJT microwave amplifier with load reflection chosen for instability 61

Chapter 1

Introduction

1.1 BACKGROUND

There is a growing interest in the analysis and design of nonlinear, microwave-frequency networks. This activity is being facilitated by the proliferation of computer-aided-design (CAD) software coupled with powerful personal computers.

Microwave circuit design and analysis are almost invariably frequency-domain in their approach. Frequency-domain formulations deal more easily with narrowband, high-frequency, distributed-parameter networks than do those in the time-domain. Indeed, the equipment available for microwave measurement—from basic directional couplers and vector voltmeters to sophisticated network analyzers—is inherently frequency-domain based. Frequency-domain representation of devices and circuits operating in the microwave region requires some form of scattering-parameter (S-parameter) characterization, as no other parameter set is suitable at these frequencies.

Nonlinear modeling, especially at microwave frequencies, poses a higher level of difficulty than does linear analysis. Because of the complexity of nonlinear models, hand calculations are generally impractical. Though there is CAD software intended for nonlinear analysis, the device models that are employed tend to be physically-based which adds to their complexity. Furthermore, the notion of S parameters to describe devices that are operating nonlinearly needs some interpretation. The S parameters are, after all, defined only for n-port networks

that obey the requirements of linearity, namely, homogeneity and superposition. There is the additional problem of creating a measurement system able to provide relatively high drive levels and independent control of the port levels such that the nonlinear element can be adequately characterized. In short, there appears to be a need for a simple, parameter-based nonlinear modeling technique that would lend itself to hand calculation or computer iteration apart from the currently available software incorporating complex device models. There is also the corresponding need for a basic measurement system for the characterization of nonlinear devices.

1.2 PREVIOUS WORK

In general, it has been difficult to obtain accurate large-signal parameters for transistors, especially at microwave frequencies. To account for the dependence of transistor parameters on the incident drive level necessitates additional complexity in the measurement system compared to the requirements for small-signal characterization. Most of the data available for microwave devices have been obtained experimentally by using some active or passive form of the "load-pull" technique [Vendelin *et al*, 1990] or by measuring so-called large-signal S parameters [Peterson *et al*, 1984]. An alternative to the latter is to extract the device S parameters at a desired operating level from a nonlinear model that is incorporated in a CAD program [Mokari-Bolhassan and Wong, 1989].

The use of load-pull techniques or S parameters to describe a nonlinear device result in the inability to predict device performance for load impedances other than the ones used for characterization. Load-pull methods have the advantage that the device can be characterized under conditions simulating actual circuit performance, but require that the measuring equipment be able to set the

load impedance to the value intended for design. The high-cost Hewlett-Packard 8510 and Wiltron 630 network analyzers are commonly used for microwave measurements, but maintaining independent control of the port levels is problematic. One approach [Khramov, 1983] involves the use of two microwave generators operating at vastly different powers in order to make the measurements. Another technique [Toropov, 1981] introduces input and output matching networks that must be adjusted such that the device-under-test, operating at a desired power level, is delivering maximum power to a load. The parameters of the device must then be de-embedded from the composite network.

The notion that the use of S parameters can be extended to nonlinear circuits goes back some twenty or more years. Extensive discussion is found in the literature of "large-signal S parameters," generally without explicit delineation of the assumptions necessary for their definition. A notable exception to this is found in a paper by Gilmore and Rosenbaum (1983). Here the authors discuss the presuppositions inherent in the quasi-linearization of S parameters: *i*) The voltages involved are nearly sinusoidal—the effects of harmonics are neglected. *ii*) The forward and reverse S parameters are functions only of the incident power at the input and output ports, respectively. The authors go on to provide an analytic approach to optimum oscillator design that is based on an active device characterized solely by its large-signal S parameters. The device modeling—done at a selection of powers incident at both ports—presumes the functional dependence of the device parameters as discussed above.

In an attempt to design a power amplifier using small-signal techniques, several researchers [Leighton *et al*, 1973] assert that a transistor's S parameters, with the exception of s_{21}, are not a strong function of excitation. The authors go on

to say that a class C power amplifier can be analyzed, at least approximately, by linear methods—a seemingly untenable claim given that the class C mode of operation is highly nonlinear. Indeed, in a later paper [van der Puije and Mazumder, 1978], the remark is made that attempts to obtain large-signal S parameters have been of limited success, especially in cases where the nonlinearity is severe such as in class C operation. Nevertheless, in an even more recent article [Hejhall, 1985], the author insists that a power amplifier design based solely on small-signal S parameters could be optimized with relative ease. This claim is made in spite of an accompanying graph showing a markedly lower efficiency at higher input power levels for a small-signal-based design relative to one using optimum source and load impedances.

In the van der Puije paper (1978), the authors propose obtaining the S parameters of a device by varying the phase of the incident wave at one port relative to the other while holding the magnitudes of both waves constant. Measurements of device reflection and transmission taken at the desired drive level over the varying phase produce circles in the complex plane, the centers of which correspond to the device S parameters.

Using a simplified unilateral physical model of a field-effect-transistor (FET) in a design of a microwave power amplifier, one researcher [Tucker, 1981] gives a method for computing the optimum load from the large-signal s_{22} as a function of device dissipation. Measured data of large-signal s_{21} are used to determine the nonlinearity in the forward gain and, using these data, the author claims that the gain-compression characteristics of the FET can be calculated for any load admittance.

1.3 PROPOSED TECHNIQUES

A calibrated measurement system is proposed that allows full two-port measurements while being excited independently at only one port. The load reflection provides the other excitation, making source switching or device reversal unnecessary. It will be shown that this technique can be utilized to accurately calibrate the measurement system. A significant advantage of the proposed measurement system essential to the characterization of nonlinear devices is that access to the load is retained. A single known standard positioned at the reference plane, two distinct lengths of transmission line for connection of the measurement ports, and three terminations—distinct, but not necessarily known—are required for calibration.

A nonlinear model is proposed that provides a full characterization of at least a certain category of nonlinear devices. The model is not merely an equivalent two-port representing a certain drive condition, but actually a representation containing information about the nonlinear function that allows prediction of the port quantities for any combination of drive levels. The model is an extension of the familiar two-port S-parameter representation of a linear network. Indeed, the equipment required for characterization is very much the same—signal generator, vector voltmeter, and directional couplers, or an equivalent four-port network analyzer. The extension to the model is the introduction of nonlinear reflection coefficients terminating additional ports with, presumably, each reflection coefficient representing a distinct two-terminal nonlinearity in a lumped-element circuit. The modeling of only a single nonlinearity will be pursued here. The nonlinear reflection coefficient is restricted to take on only real values which facilitates its characterization and utilization.

1.4 ORGANIZATION OF THESIS

The succeeding chapters of this thesis are organized in the following way: Chapter 2 contains a review of current calibration schemes along with a detailed description of the proposed one-way, two-port measurement system. Chapter 3 contains a discussion of the proposed nonlinear model and a detailed procedure for computing the model parameters. Chapter 4 shows the application of the nonlinear model to the prediction of amplifier gain over varying drive level. An approach to oscillator design is also given. Chapter 5 provides a summary of the objectives and results of the thesis.

Chapter 2

Calibration

2.1 INTRODUCTION

Microwave S-parameter measurements involving the use of a network analyzer or vector voltmeter are subject to systematic, or repeatable, errors that are generally the most significant source of measurement uncertainty. These errors include mismatch and leakage in the test setup, imperfect isolation between the reference and test signal paths, and variations in system response with frequency. Because these errors are predictable, their effects can be removed from the measured data in order to obtain corrected values for the response of the device under test (DUT). Therefore, before actual device measurements are made, a calibration process is performed to characterize these errors.

In practice, calibration requires the measurement of the magnitude and phase responses of known standard devices and the use of these data in conjunction with a model of the measurement system to determine error contributions. The DUT is then measured and vector mathematics is employed to compute the actual response of the DUT by removing the error contributions. The results are limited by the dynamic range of the instrument, by the extent to which the characteristics of the calibration standards are known, and by system noise or random errors.

The particular model chosen to describe the measurement system determines the method of calibration, with the complexity of the model being a function of the number of error terms to be included. A brief summary of a number of common calibration models is presented along with signal flow-graphs for model

representation. A new one-way, two-port calibration system is then described. This latter system was developed to make the necessary measurements of nonlinear devices for the characterization of a nonlinear model proposed in the next chapter.

2.2 ONE-PORT MODELS

Simple one-port system models [Rytting, 1982] can be used when only reflection measurements are to be made on the device. See Fig. 2.1. In the simplest calibration, a "response" model is used. The error terms e_{00} and e_{11}, corresponding to system directivity (isolation) and port match, respectively, are set to zero. Forward response error e_{01} is determined by connecting a standard of known reflection coefficient Γ at precisely the electrical point where the DUT will subsequently be positioned. (This point is known as the measurement plane.) Because it is relatively simple to construct, the reflection standard is typically a short having $\Gamma = -1$. Then, the measured reflection, $\Gamma_m \equiv \frac{b_1'}{a_1'}$, gives $e_{01} = \frac{\Gamma_m}{\Gamma}$.

If the model includes the isolation term e_{00}, a termination having $\Gamma = 0$, hereafter called a load, is connected, and $e_{00} = \Gamma_m$. Then another standard is connected (again typically a short) and $e_{01} = \frac{\Gamma_m - e_{00}}{\Gamma}$ where Γ_m and Γ now correspond to the measured and assumed reflection, respectively, of the second standard.

For the full one-port model, three distinct standards are required. As for the response model, e_{00} is found using a load standard. Then two additional standards are used to obtain e_{01} and e_{11}, typically an "open" (a lossless termination having approximately zero phase) and a short. If the load standard is not perfect ($\Gamma \neq 0$), but is known, the error terms are found by solving the set of three equations obtained from measurements of the three standards and the use of the model flow-

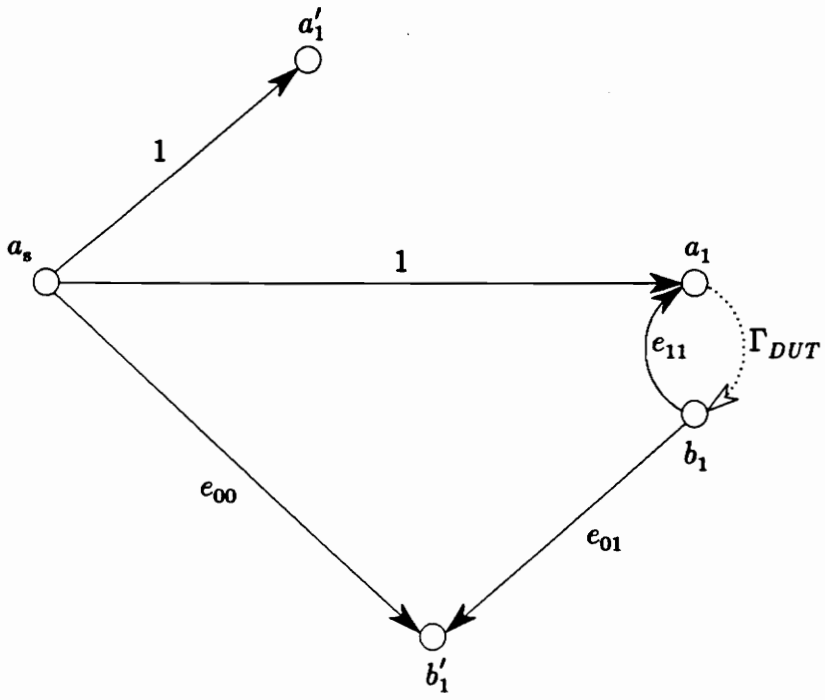

Figure 2.1. One-port calibration model for microwave S-parameter measurements.

graph-derived expression $\Gamma_m = e_{00} + \frac{e_{01}\Gamma}{1 - e_{11}\Gamma}$. This procedure is commonly called "Open-Short-Load" (OSL), though the three standards need only be distinct and known.

2.3 TWO-PORT MODELS

Two-port system models [Rytting, 1982] allow transmission as well as reflection measurements to be made. There are three distinct two-port calibration procedures currently established in the literature, and a fourth process which is a slight modification.

If a two-port test-set is not available with the option to switch the signal source to either port, a one-way two-port model (Fig. 2.2) can be utilized with the DUT turned around to make the reverse measurements. Error terms e_{00}, e_{01} and e_{11} are determined in the same manner as in the one-port case. System crosstalk (isolation), represented by e_{30}, is measured with port 1 terminated in a load and with no connection at port 2, giving $e_{30} = \tau_m$, where τ_m is the measured transmission, $\tau_m \equiv \frac{b_2'}{a_1'}$.

Port 1 and port 2 are then connected, either directly or with a short length of transmission line; this procedure is known as inserting a Thru. The port 2 match term, e_{22}, is then measured as a one-port load, giving $e_{22} = \Gamma_m$. Finally, the port 2 response error, e_{32}, is calculated as $e_{32} = (\tau_m - e_{30})(1 - e_{11}e_{22})$. With all the model error terms determined, the composite S parameters of a DUT can be measured, $s_{21}' \equiv \tau_m$ and $s_{11}' \equiv \Gamma_m$ in the forward direction and, equivalently, $s_{12}' \equiv \tau_m$ and $s_{22}' \equiv \Gamma_m$ with the DUT reversed. From the error model, four linear equations can be derived relating the actual device parameters to the composite measurements and the model error terms. The closed-form solutions to these equations are

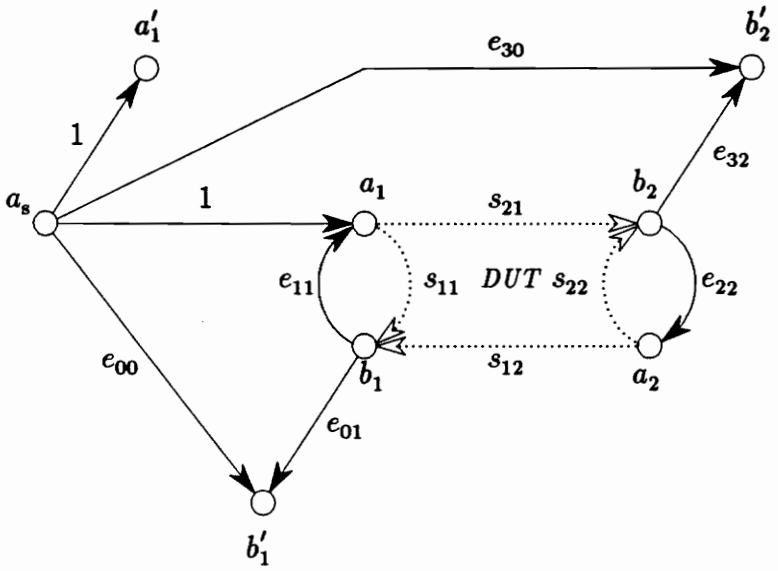

Figure 2.2. Two-port calibration model for microwave S-parameter measurements.

available in the literature [Kasa, 1974].

A full two-port calibration system can be obtained by simply determining the above one-way model for both forward (port 1) and reverse (port 2) excitation. Generally, no attempt is made to link the two models. After the error terms are found, measurements are made of the DUT composite parameters (now without reversing the DUT). Again, the result is four equations which can be solved for the device parameters.

The method of Thru-Reflect-Line (TRL) [Engen and Hoer, 1979] is an alternate approach to two-port calibration that relies on transmission lines instead of discrete impedance standards. Although the application of TRL results in the same error correction as in the conventional full two-port model, the mathematical derivation differs. Thru and system isolation measurements are the same as in the full two-port method. Line measurements are identical to those using the Thru but employ a connection of different length between ports 1 and 2. (The characteristic impedance of the Line becomes the standard impedance of the system.) TRL also uses a reflection standard, typically an open or short, with which the reflection coefficient of each test port is measured. Additional correction is provided by measuring the ratio of the test-set incident signals during the Thru and Line steps and modifying the e_{11} and e_{22} port match terms in order to account for any differences in the two sources.

The Thru-Reflect-Match (TRM) method [Barr and Pervere, 1989; Eul and Schiek, 1988] simply replaces the Line step of TRL with matched load terminations at port 1 and port 2. The load terminations appear to the measurement system as the connection of a Line having an infinite attenuation.

2.4 PROPOSED ONE-WAY TWO-PORT MODEL

Consider the calibration model [Davis, 1991] shown in Fig. 2.3. This system differs in several ways from those outlined above: First, full two-port measurements can be made without necessitating source switching or device reversal. Second, in contrast with a typical network analyzer setup for S-parameter measurements, this system retains access to the load presented to the DUT, and the option is available to use a high-power generator for large-signal measurements. Finally, the requirements for calibration are a single known standard positioned at the reference plane, a Thru and Line connecting ports 1 and 2, and three distinct terminations located at the system output. The details of calibration are given in the following sections.

2.4.1 Reflection

From the model flow-graph, the measured reflection Γ_m ($\equiv \frac{b_1'}{a_1'}$) is

$$\Gamma_m = e_{00} + \frac{e_{01}\Gamma}{1 - e_{11}\Gamma} = \frac{e_{00} - (e_{00}e_{11} - e_{01})\Gamma}{1 - e_{11}\Gamma} \ , \tag{2.1}$$

where Γ is the reflection coefficient at the reference plane. The above equation, bilinear in Γ, can be rewritten with the error terms a, b, and d as new constants to give

$$\Gamma_m = \frac{a + b\Gamma}{1 + d\Gamma} \ , \tag{2.2}$$

where

$$a = e_{00} \tag{2.3a}$$

$$b = -(e_{00}e_{11} - e_{01}) \tag{2.3b}$$

$$d = -e_{11} \ . \tag{2.3c}$$

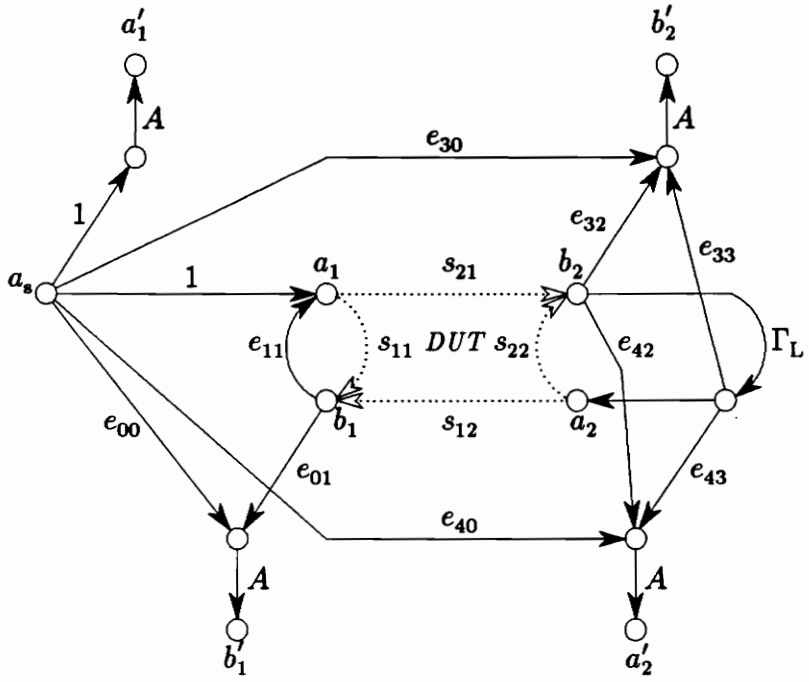

PROPOSED ONE-WAY TWO-PORT MODEL

Figure 2.3. Proposed one-way two-port calibration model for microwave *S*-parameter measurements.

In solving for the above variables, one known standard is used, with the measurement system reference plane determined by the standard's electrical position. A reflection measurement is made of this standard connected at port 1. Subsequent reflection measurements are taken of three terminations at the system output with a Thru and a Line successively connected between ports 1 and 2. The three terminations may not necessarily be known, but they must be distinct, as must be the electrical lengths of the Thru and Line. The measurements are used to write seven independent equations of the form of (2.2) which after some manipulation yield values for the error terms. The details of the procedure are now presented.

The calibration procedure begins with the reflection measurement of the standard connected at port 1. The first equation is written as

$$\Gamma_{sm} = \frac{a + b\Gamma_s}{1 + d\Gamma_s} \ , \tag{2.4}$$

where the value of standard Γ_s must be known. Typically, the standard is a short ($\Gamma_s = -1$), in which case

$$\Gamma_{sm} = \frac{a - b}{1 - d} \ . \tag{2.4a}$$

The Thru is then used to connect port 1 to port 2 and one of the three terminations is connected to the system output. A reflection measurement now yields

$$\Gamma_{1t} = \frac{a + b\Gamma_1}{1 + d\Gamma_1} \ ,$$

where Γ_1 is the reflection at the reference plane corresponding to the first termination and Γ_{1t} is a measured quantity. Measurement of the same termination

using the Line instead of the Thru produces

$$\Gamma_{1l} = \frac{a + b\Gamma_1 x}{1 + d\Gamma_1 x} \ ,$$

where x is the delay parameter representing the electrical length difference between the Thru and Line.

Similarly, four additional equations can be written from the measurements of the remaining two terminations. The general form of the equations resulting from the measurements using the Thru and Line can be written as

$$\Gamma_{it} + d\Gamma_{it}\Gamma_i - a - b\Gamma_i = 0 \tag{2.5a}$$

$$\Gamma_{il} + d\Gamma_{il}\Gamma_i x - a - b\Gamma_i x = 0 \ . \tag{2.5b}$$

Combining (2.5a) and (2.5b) to eliminate Γ_i and writing out the result for each termination gives

$$(\Gamma_{1l} - a)(\Gamma_{1t} d - b) = x(\Gamma_{1t} - a)(\Gamma_{1l} d - b) \tag{2.6a}$$

$$(\Gamma_{2l} - a)(\Gamma_{2t} d - b) = x(\Gamma_{2t} - a)(\Gamma_{2l} d - b) \tag{2.6b}$$

$$(\Gamma_{3l} - a)(\Gamma_{3t} d - b) = x(\Gamma_{3t} - a)(\Gamma_{3l} d - b) \ . \tag{2.6c}$$

Eliminating delay parameter x by combining (2.6a) and (2.6b) results in

$$[\Gamma_{2t}\Gamma_{2l}(\Gamma_{1t} - \Gamma_{1l}) - \Gamma_{1t}\Gamma_{1l}(\Gamma_{2t} - \Gamma_{2l})] =$$
$$[(\Gamma_{2t} - \Gamma_{2l}) - (\Gamma_{1t} - \Gamma_{1l})]\frac{ab}{d} + [\Gamma_{1t}\Gamma_{2l} - \Gamma_{2t}\Gamma_{1l}]\frac{ad + b}{d} \ . \tag{2.7a}$$

Similarly combining (2.6b) and (2.6c) gives

$$[\Gamma_{2t}\Gamma_{2l}(\Gamma_{3t}-\Gamma_{3l})-\Gamma_{3t}\Gamma_{3l}(\Gamma_{2t}-\Gamma_{2l})]= [(\Gamma_{2t}-\Gamma_{2l})-(\Gamma_{3t}-\Gamma_{3l})]\frac{ab}{d}+[\Gamma_{3t}\Gamma_{2l}-\Gamma_{2t}\Gamma_{3l}]\frac{ad+b}{d} \quad . \tag{2.7b}$$

Now, by combining (2.7a) and (2.7b), the unknowns $\frac{ab}{d}$ and $\frac{ad+b}{d}$ can be determined in terms of the measured reflections as

$$\frac{ab}{d}=\frac{\alpha}{\gamma} \tag{2.8a}$$

$$\frac{ad+b}{d}=\frac{\beta}{\gamma} \quad , \tag{2.8b}$$

where

$$\alpha=\Gamma_{1t}\Gamma_{1l}(\Gamma_{3t}\Gamma_{2t}-\Gamma_{2t}\Gamma_{3l})+\Gamma_{2t}\Gamma_{2l}(\Gamma_{3l}\Gamma_{1t}-\Gamma_{3t}\Gamma_{1l})+\Gamma_{3t}\Gamma_{3l}(\Gamma_{2t}\Gamma_{1l}-\Gamma_{1t}\Gamma_{2l})$$

$$\beta=\Gamma_{1t}\Gamma_{1l}(\Gamma_{3t}-\Gamma_{3l}-(\Gamma_{2t}\Gamma_{2l}))+\Gamma_{2t}\Gamma_{2l}(\Gamma_{1t}-\Gamma_{1l}-(\Gamma_{3t}-\Gamma_{3l}))+ \Gamma_{3t}\Gamma_{3l}(\Gamma_{2t}-\Gamma_{2l}-((\Gamma_{1t}-\Gamma_{1l}))$$

$$\gamma=\Gamma_{1t}(\Gamma_{2l}-\Gamma_{3l})+\Gamma_{2t}(\Gamma_{3l}-\Gamma_{1l})+\Gamma_{3t}(\Gamma_{1l}-\Gamma_{2l}) \quad .$$

Equations (2.8a) and (2.8b) can be rearranged and combined to give

$$a^2-\frac{\beta}{\gamma}a+\frac{\alpha}{\gamma}=0 \tag{2.9a}$$

and

$$\left(\frac{b}{d}\right)^2-\frac{\beta}{\gamma}\left(\frac{b}{d}\right)+\frac{\alpha}{\gamma}=0 \quad . \tag{2.9b}$$

The general form of (2.9a) and (2.9b) is

$$y^2 - \frac{\beta}{\gamma} y + \frac{\alpha}{\gamma} = 0 \quad , \tag{2.10}$$

where the roots y_1 and y_2 are self-evident as

$$\begin{aligned} y_1 &= a \\ &\equiv e_{00} \quad \text{from (2.3a)} \end{aligned} \tag{2.11a}$$

and

$$\begin{aligned} y_2 &= \frac{b}{d} \\ &\equiv \frac{e_{00}e_{11} - e_{01}}{e_{11}} \quad \text{from (2.3b) and (2.3b)} \, . \end{aligned} \tag{2.11b}$$

Error term e_{00}, which represents effective directivity (the sum of all leakage signals appearing at b_1), is expected to be small and therefore is equated to the smaller root of (2.10).

Before the familiar quadratic formula is applied to (2.10), the possibility is considered of γ approaching zero and, consequently, the ratios $\frac{\alpha}{\gamma}$ and $\frac{\beta}{\gamma}$ approaching infinity. Thus, (2.10) is first rewritten as

$$\gamma y^2 - \beta y + \alpha = 0 \tag{2.12}$$

and (2.12) is then multiplied by y^{-2} to become

$$\alpha y^{-2} - \beta y^{-1} + \gamma = 0 \quad . \tag{2.13}$$

The quadratic formula is applied to (2.13) and y_1 is found as

$$e_{00} = y_1 = \frac{2\alpha}{\beta \pm \sqrt{\beta^2 - 4\gamma\alpha}} \quad , \tag{2.14}$$

where the sign in the denominator is chosen for the root with the smaller magnitude. The form of (2.14) is well-behaved for small γ, as desired. The second root (2.11b) is found in reciprocal form as

$$\frac{1}{y_2} = \frac{e_{11}}{e_{00}e_{11} - e_{01}} = \frac{2\gamma}{\beta \pm \sqrt{\beta^2 - 4\gamma\alpha}} \quad , \tag{2.15}$$

where the sign in the denominator is chosen for the ratio having the smaller magnitude.

Solving for error e_{11}, using (2.3c) and a rearrangement of (2.4a), results in

$$e_{11} = -d = \frac{\frac{d}{b}(a - \Gamma_{sm})}{\frac{d}{b}\Gamma_{sm} - 1} \quad , \tag{2.16}$$

where a is known from (2.11a) and (2.14) and $\frac{d}{b}$ is known from (2.11b) and (2.15).

With e_{00} and e_{11} known, e_{01} may be solved for by using (2.3a), (2.3b), and (2.3c) in (2.4) to give

$$e_{01} = \frac{(\Gamma_{sm} - e_{00})(1 - e_{11}\Gamma_s)}{\Gamma_s} \tag{2.17}$$

2.4.2 Isolation

The measurement system isolation (crosstalk) terms, e_{30} and e_{40}, are found with port 1 terminated in a load and no connection at port 2. Then

$$e_{30} = \tau_m$$

and

$$e_{40} = r_m \quad ,$$

where r_m is the measured source ratio, $r_m \equiv \frac{a_2'}{a_1'}$. If the magnitudes of the crosstalk terms approximate the reading of the measurement instrument with its probes removed from the test ports, then e_{30} and e_{40} are simply set to zero.

2.4.3 Transmission

With e_{00}, e_{01}, e_{11}, e_{30}, and e_{40} known, the remaining model error terms can be determined. Port 1 and port 2 are connected with a Thru, and measurements are made of reflection, transmission, and source ratio with two distinct terminations. A subset of the three terminations employed in Section 2.4.1 is used in order to avoid additional reflection measurements. From the model flow-graph, the measured reflection, transmission, and source ratio are given, respectively, as

$$\Gamma_m = e_{00} + \frac{e_{01}\Gamma_L}{1 - e_{11}\Gamma_L} \tag{2.18}$$

$$\tau_m = e_{30} + \frac{e_{32} + e_{33}\Gamma_L}{1 - e_{11}\Gamma_L} \tag{2.19}$$

$$r_m = e_{40} + \frac{e_{42} + e_{43}\Gamma_L}{1 - e_{11}\Gamma_L} \quad , \tag{2.20}$$

where Γ_L is the reflection coefficient at the reference plane corresponding to a given termination at the system output. Equations (2.18) through (2.20) are rearranged, respectively, as

$$\Gamma_L = \frac{e_{00} - \Gamma_m}{(e_{00}e_{11} - e_{01}) - e_{11}\Gamma_m} \tag{2.21}$$

$$(\tau_m - e_{30})(1 - e_{11}\Gamma_L) = e_{32} + e_{33}\Gamma_L \tag{2.22}$$

$$(r_m - e_{40})(1 - e_{11}\Gamma_L) = e_{42} + e_{43}\Gamma_L \quad . \tag{2.23}$$

From the measured reflections of the two terminations, two values of Γ_L are calculated using (2.21). These values are then used in (2.22) and (2.23) to create four equations in four unknowns which are solved for the remaining error terms.

2.5 DEVICE MEASUREMENTS

With all the error terms of the measurement system now known, the input reflection and transmission of the DUT may be determined along with the actual load reflection. In general, with a DUT connected at the reference plane, the *measured* reflection, transmission, and source ratio are given, respectively, as

$$\Gamma_m = e_{00} + \frac{e_{01}\Gamma}{1 - e_{11}\Gamma} \tag{2.24}$$

$$\tau_m = e_{30} + \frac{\tau(e_{32} + e_{33}\Gamma_L)}{1 - e_{11}\Gamma} \tag{2.25}$$

$$r_m = e_{40} + \frac{\tau(e_{42} + e_{33}\Gamma_L)}{1 - e_{11}\Gamma} \quad , \tag{2.26}$$

where Γ and τ are the true input reflection and transmission of the DUT, respectively, and Γ_L is the actual load reflection presented to the DUT. Using (2.24) to solve for Γ results in

$$\boxed{\Gamma = \frac{e_{00} - \Gamma_m}{(e_{00}e_{11} - e_{01}) - e_{11}\Gamma_m}} \quad . \tag{2.27}$$

It is useful to have a means of determining Γ_L without removing the DUT and inserting a Thru. The uncorrected load reflection, Γ'_L,—the ratio of a'_2 to b'_2 with only the crosstalk error contributions removed—is

$$\Gamma'_L = \frac{a'_2 - e_{40}a'_1}{b'_2 - e_{30}a'_1} = \frac{\frac{a'_2}{a'_1} - e_{40}}{\frac{b'_2}{a'_1} - e_{30}} \quad . \tag{2.28a}$$

With the use of (2.19) and (2.20) in (2.28a), Γ'_L is written as

$$\Gamma'_L = \frac{r_m - e_{40}}{\tau_m - e_{30}} \quad , \tag{2.28b}$$

where the quantities r_m and τ_m can be measured with a DUT at the reference plane. Γ'_L is related to the actual load reflection, Γ_L, by substituting (2.25) and (2.26) into (2.28b) to give

$$\Gamma'_L = \frac{e_{42} + e_{43}\Gamma_L}{e_{32} + e_{33}\Gamma_L} \quad . \tag{2.29}$$

Solving (2.29) for Γ_L results in

$$\boxed{\Gamma_L = \frac{e_{42} - e_{32}\Gamma'_L}{-e_{43} + e_{33}\Gamma'_L}} \quad . \tag{2.30}$$

With Γ and Γ_L known, the value of τ may be found using (2.25):

$$\boxed{\tau = \frac{(\tau_m - e_{30})(1 - e_{11}\Gamma)}{e_{32} + e_{33}\Gamma_L}} \quad . \tag{2.31}$$

In general, it is necessary to record the input drive to the DUT when making level-dependent measurements of reflection and transmission. The drive level at the

DUT is

$$\boxed{a_1 = \frac{Aa_1'}{1 - e_{11}\Gamma}} \quad , \tag{2.32}$$

where

$$A \equiv \left.\frac{a_1}{a_1'}\right|_{\Gamma_L=0} \quad . \tag{2.33}$$

2.6 *S*-PARAMETER MEASUREMENTS

The S parameters of the DUT can be determined by measuring the device reflection, Γ, and transmission, τ, for two distinct values of load reflection, Γ_L, circumventing the need to independently control the level at a_2.

From the device flow-graph, reflection and transmission are defined, respectively, as

$$\Gamma = s_{11} + \frac{s_{21}s_{12}\Gamma_L}{1 - s_{22}\Gamma_L} \tag{2.34}$$

and

$$\tau = \frac{s_{21}}{1 - s_{22}\Gamma_L} \quad . \tag{2.35}$$

Rewritting (2.35) for each load reflection gives

$$s_{21} = \tau_1(1 - s_{22}\Gamma_{L1}) \tag{2.36}$$

$$s_{21} = \tau_2(1 - s_{22}\Gamma_{L2}) \tag{2.37}$$

and equating (2.36) and (2.37) to eliminate s_{21} results in

$$\boxed{s_{22} = \frac{\tau_1 - \tau_2}{\tau_1\Gamma_{L1} - \tau_2\Gamma_{L2}}} \quad . \tag{2.38}$$

Substituting (2.38) in (2.36) or (2.37) results in

$$\boxed{s_{21} = \frac{\tau_1 \tau_2 (\Gamma_{L1} - \Gamma_{L2})}{\tau_1 \Gamma_{L1} - \tau_2 \Gamma_{L2}}} \quad . \tag{2.39}$$

To find s_{12}, (2.34) is rewritten for each load reflection. The two equations are combined to eliminate s_{11}, and (2.38) and (2.39) are substituted for s_{22} and s_{21} to give

$$\boxed{s_{12} = \frac{\Gamma_1 - \Gamma_2}{\tau_1 \Gamma_{L1} - \tau_2 \Gamma_{L2}}} \quad . \tag{2.40}$$

Finally, (2.35) is used in (2.34) to write

$$s_{11} = \Gamma_1 - \tau_1 s_{12} \Gamma_{L1} \quad , \tag{2.41}$$

which upon substitution of (2.40) becomes

$$\boxed{s_{11} = \frac{\tau_1 \Gamma_{L1} \Gamma_2 - \tau_2 \Gamma_{L2} \Gamma_1}{\tau_1 \Gamma_{L1} - \tau_2 \Gamma_{L2}}} \quad . \tag{2.42}$$

Chapter 3

Nonlinear Model

3.1 INTRODUCTION

Microwave circuit design involving the large-signal operation of an active device requires accurate device characterization that poses complications over those encountered in small-signal modeling. Extensive lumped- and distributed-element physical models, while offering a strong relationship to device physics, necessitate the use of large-scale computer-aided-design (CAD) software. Other methods that rely on an S-parameter-based model require, because of the nonlinear behavior of the device, numerous measurements made at varying power levels and terminating impedances. Thus there is the motivation for the development of a hybrid approach to large-signal modeling in which a parameter-based model that describes the linear behavior of the device is combined with a circuit-based component to account for the nonlinear effects.

Consider the possibility of representing a nonlinear circuit by a standard two-port S-parameter model with one extension: additional ports coupled to the first two, and terminated in devices having nonlinear reflection coefficients [Davis and Keller, 1991]. Furthermore, consider restricting the nonlinear reflections to be memoryless, that is, point-by-point functions independent of time. In the frequency domain, this restriction implies that the nonlinear functions would assume only real values, making possible their easy characterization and utilization. Interaction between the nonlinear reflections and the complex-valued linear subnetwork in the phasor domain allows not only a change in the amplitude response but also the

appropriate change in phase response.

Presumably, every two-terminal nonlinearity in a lumped-element circuit would be represented as a nonlinear reflection in an S-parameter model of that circuit. For simplicity, however, it will be assumed here that only one significant nonlinearity is present. In the model of a non-saturated bipolar junction transistor (BJT), for example, a single nonlinear device would represent the base-emitter junction, with the other components of the model representing the transistor's linear elements. Experimental work with BJT's demonstrated that a single, memoryless nonlinearity, embedded in a three-port flow-graph, is indeed sufficient to represent the behavior of common devices.

There are several advantages to this proposed model. The only drive-dependent element is the single nonlinearity which is easily determined from measurement; only two load impedances are needed for characterization. After characterization, model behavior can then be predicted for any load or source termination and thus the model lends itself well to common design problems with varied terminations. For example, the model may be used to determine the transmission and input and output reflection of an amplifier design. Also, the model is simple and degenerates to the familiar two-port flow-graph for small-signal analysis. In short, the majority of the flow-graph is linear and constant and the nonlinear portion is known in tabular or graphical form. These parts combine to produce a fully determined model.

The model will be limited here to narrowband, fixed-frequency, and fixed-bias-configuration circuits dominated by a single nonlinearity. Application of the model will require that device saturation be avoided due to the single nonlinearity assumption. Furthermore, the prediction of harmonic generation will not be

considered.

3.2 MODEL REPRESENTATION

The proposed model is shown in Fig. 3.1. The nonlinearity is embedded in the model as the reflection coefficient Γ_N located at port 3. The value of Γ_N is a nonlinear function of the drive level at port 3 and is constrained to take on only real values. Thus Γ_N represents a purely resistive (or memoryless) circuit element. At drive levels corresponding to small-signal conditions, Γ_N is assumed to be zero. The balance of the model is considered to be a linear, time-invariant network.

From the model flow-graph, the input reflection Γ ($\equiv \frac{b_1}{a_1}$) and the transmission τ ($\equiv \frac{b_2}{a_1}$) are found as

$$\Gamma = s_{11} + \frac{s_{13}s_{31}\Gamma_N(1 - s_{22}\Gamma_L) + s_{21}s_{12}\Gamma_L(1 - s_{33}\Gamma_N) + s_{31}s_{23}s_{12}\Gamma_N\Gamma_L}{1 - s_{22}\Gamma_L - s_{33}\Gamma_N - (s_{23}s_{32} - s_{22}s_{33})\Gamma_N\Gamma_L} \tag{3.1}$$

and

$$\tau = \frac{s_{21}(1 - s_{33}\Gamma_N) + s_{31}s_{23}\Gamma_N}{1 - s_{22}\Gamma_L - s_{33}\Gamma_N - (s_{23}s_{32} - s_{22}s_{33})\Gamma_N\Gamma_L} \quad , \tag{3.2}$$

where Γ_L ($\equiv \frac{a_2}{b_2}$) is the load reflection coefficient at port 2.

In (3.1) and (3.2), the expressions for Γ and τ are both bilinear transformations of the variable Γ_N. From complex variable theory it is known that bilinear transformations always transform circles into circles. As Γ_N has been constrained to be real, the values it assumes will fall on a straight line. A line can be considered as a degenerate case of a circle, that is, a circle having an infinite radius and center. Thus for a range of values of Γ_N, corresponding to a range of excitations, the quantities Γ and τ have the locus of a circle.

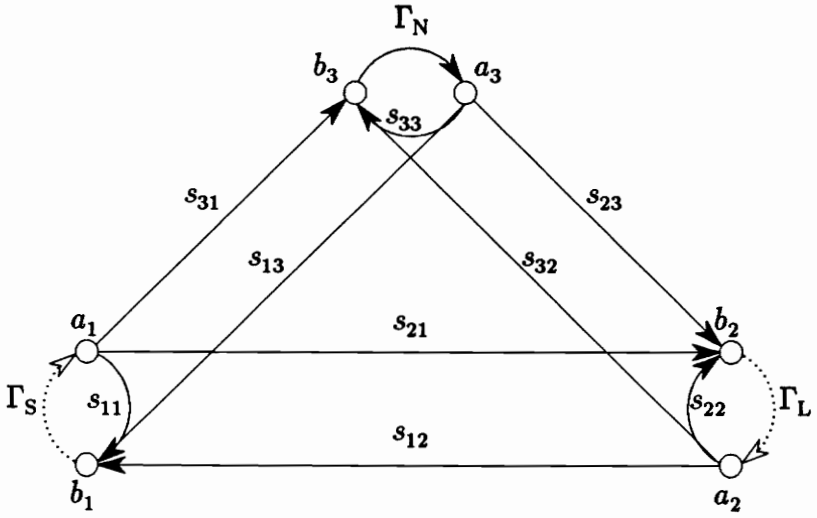

NONLINEAR MODEL

Figure 3.1. Model for representation of two-port device having a single, memoryless nonlinearity.

The fact that the values of Γ and τ corresponding to different drive levels have the locus of circles will be needed in the next section to determine the model parameters. By measuring at least three points that are known to fall on a circle, the center and radius of that circle can be determined—a larger number of measurements not being necessary. If a few noise-free measurements are made and there is confidence in the applicability of the model, then the few measurements are sufficient to determine the circle.

There may be instances where a larger number of drive level measurements would be desirable to ensure good circle-fitting. And, indeed, it must be noted that a larger number of measurements *are* necessary in order to fully characterize the nonlinear element of the model. However, the change in drive level is one-dimensional—the reflection coefficient of the chosen load termination along with the effects of the model network fix the a_1 to a_2 relationship. Under this condition and with the knowledge that the measurement values must lie on a circle, model parameters can be found which will make possible the prediction of model behavior for any combination of a_1 and a_2 in a complex phasor sense. Thus the characterization of the model in one dimension is extended to two, that is, from a_1 and a_2 having a fixed relationship to a_1 and a_2 assuming any values. In other words, instead of the equivalent two-port flow paths being determined, the nonlinear element itself is characterized.

3.3 DETERMINATION OF MODEL PARAMETERS

Before the model parameters of the device-under-test (DUT) can be determined, the measurement system should be calibrated using the procedure detailed in Chapter 2. All quantities that follow assume a calibrated measurement

system.

In order to characterize the model, it is necessary to make measurements of Γ and τ over a range of input drive levels and with two distinct load terminations, hereafter called Γ_{L1} and Γ_{L2}. As discussed above, even though data at only three different levels are required for the determination of the linear portion of the model, supplemental measurements at other drive levels are necessary for the characterization of the nonlinear element. The additional measurements may also be desirable to overcome the effects of system noise and improve the subsequent circle fitting.

3.3.1 Small-Signal

For the model to represent the DUT operating in a small-signal mode, the model nonlinearity, Γ_N, is equated to zero and the model flow-graph becomes a two-port. To determine the small-signal model parameters, the drive level applied to the DUT must be set low enough to ensure linear operation. Input reflection and transmission data for the DUT are obtained using each of the two loads. The formulas developed in Section 2.6—(2.42), (2.40), (2.39), and (2.38)—are then utilized to obtain

$$s_{11} = \frac{\tau_1\Gamma_{L1}\Gamma_2 - \tau_2\Gamma_{L2}\Gamma_1}{\tau_1\Gamma_{L1} - \tau_2\Gamma_{L2}} \ ,$$

$$s_{12} = \frac{\Gamma_1 - \Gamma_2}{\tau_1\Gamma_{L1} - \tau_2\Gamma_{L2}} \ ,$$

$$s_{21} = \frac{\tau_1\tau_2(\Gamma_{L1} - \Gamma_{L2})}{\tau_1\Gamma_{L1} - \tau_2\Gamma_{L2}} \ ,$$

$$s_{22} = \frac{\tau_1 - \tau_2}{\tau_1\Gamma_{L1} - \tau_2\Gamma_{L2}} \ .$$

3.3.2 Choice of S_{33}

To begin solving for the large-signal model parameters, circles are fit to the points corresponding to either the transmission or reflection data for each load reflection. The circle-fitting procedure given by Kasa (1976) uses a modified least-square-error criterion to effect a closed-form solution. Circles fitted to transmission and reflection data for a microwave transistor amplifier operating at 880 MHz are shown in Figs. 3.2 and 3.3, respectively. When these data were recorded, care was taken to limit the input drive level to prevent device saturation. The effect of a further increase in the drive level is illustrated in Figs. 3.4 and 3.5. (In each of the circle plots, the origin is located at the center of the enclosed rectangular area, which accounts for the location of the circle.) As device saturation begins to occur, the departure of the measured data from the original circle curvature may be observed, particularly in the case of reflection. The resulting fitted circles, consequently, have centers that are invalid for device characterization. The discussion here continues with the assumption that transmission data that has been drive-level limited is used for circle-fitting.

The circle that has been fitted to the transmission data passes through a point corresponding to small-signal transmission. Thus, if the small-signal component is removed from each data point, the fitted circle must pass through the origin. The general parametric form for a circle in the complex plane versus θ is

$$z = C \pm Re^{j\theta} \quad , \tag{3.3}$$

where C and R are the center and radius. The circle representing only large-signal transmission—thus passing through the origin—has a radius equal to the

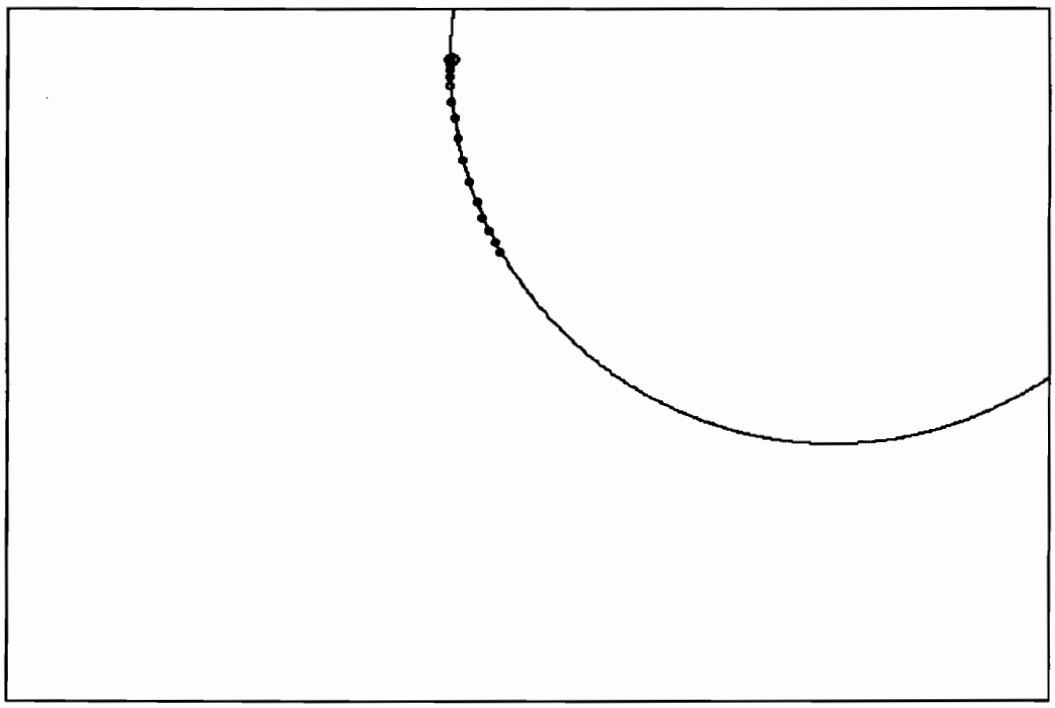

TRANSMISSION CIRCLE

Figure 3.2. Circle fit to transmission data points. Input drive level limited to prevent saturation of device under test.

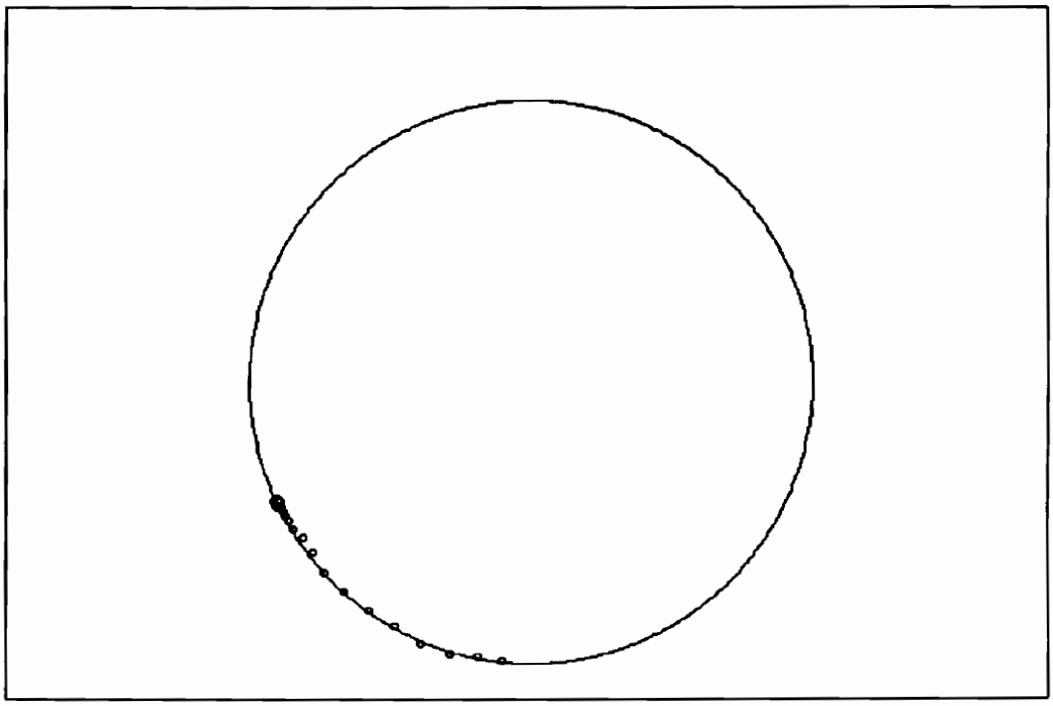

REFLECTION CIRCLE

Figure 3.3. Circle fit to reflection data points. Input drive level limited to prevent saturation of device under test.

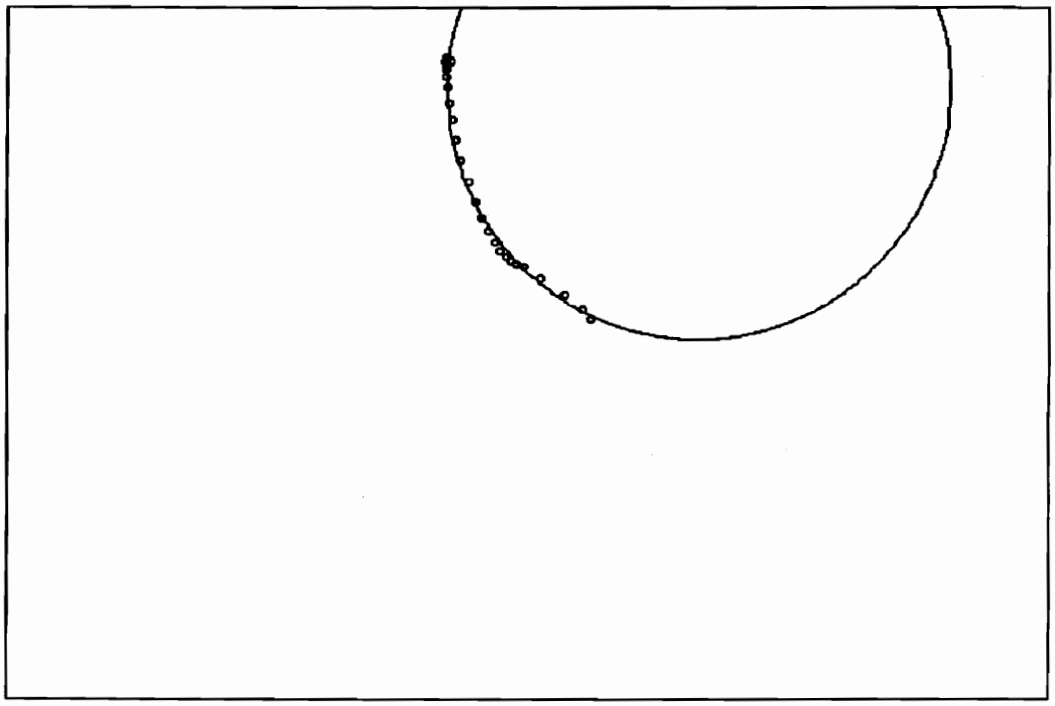

Figure 3.4. Circle fit to transmission data points. Input drive level becoming sufficiently high to saturate device under test.

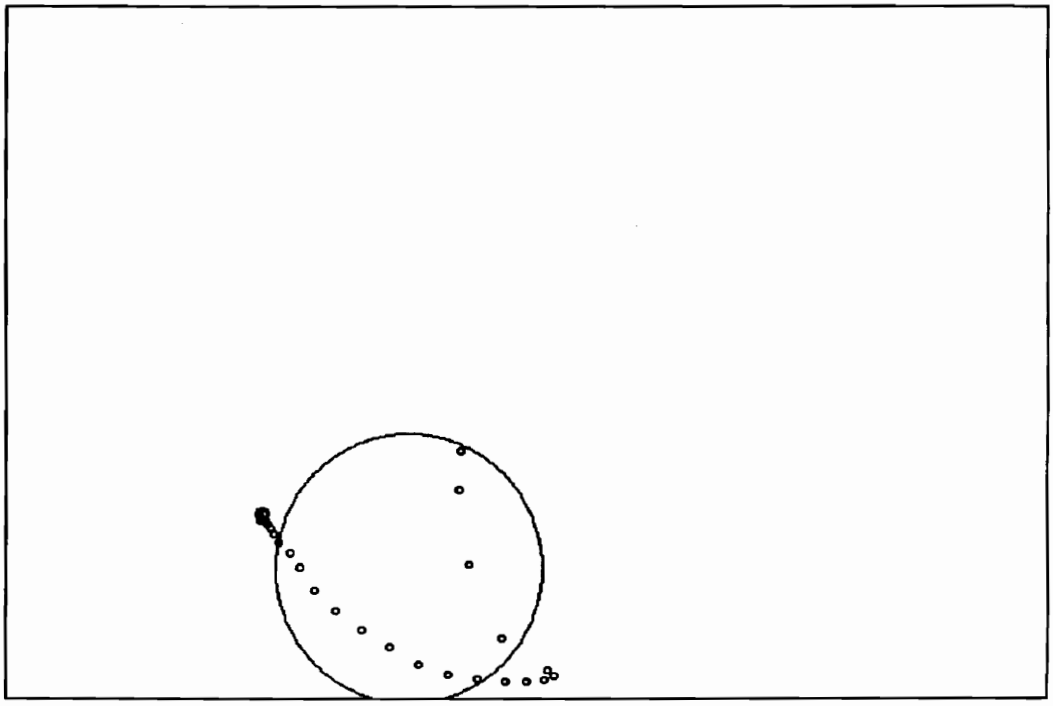

REFLECTION CIRCLE

Figure 3.5. Circle fit to reflection data points. Input drive level becoming sufficiently high to saturate device under test.

magnitude of its center:

$$\tau - \tau_0 = C_\tau \pm |C_\tau| e^{j\theta} \quad , \tag{3.4}$$

where C_τ is the center of the large-signal transmission circle and τ_0 is the small-signal transmission. In (3.4), $|C_\tau|$ is replaced by the complex quantity C_τ with the additional phase component absorbed by the angle of the complex exponential to give, without loss of generality,

$$\tau - \tau_0 = C_\tau \pm C_\tau e^{j\phi} \quad . \tag{3.5}$$

Because (3.5) must be true for any load reflection, the choice is made to write the large-signal transmission in terms of the model paths for a load reflection of zero as

$$(\tau - \tau_0)\Big|_{\Gamma_L=0} = \frac{s_{23}s_{31}\Gamma_N}{1 - s_{33}\Gamma_N} \quad . \tag{3.6}$$

Now, the right sides of (3.5) (choosing the minus sign) and (3.6) are equated and rearranged to solve for $e^{j\phi}$ as

$$e^{j\phi} = \frac{1 - \left(\frac{s_{33}C_\tau + s_{23}s_{31}}{C_\tau}\right)\Gamma_N}{1 - s_{33}\Gamma_N} \quad . \tag{3.7}$$

Since the magnitude of the expression on the right side of (3.7) must be unity and Γ_N is assumed to be real, the coefficients of Γ_N must be conjugates:

$$\frac{s_{33}C_\tau + s_{23}s_{31}}{C_\tau} = s_{33}^* \quad . \tag{3.8}$$

Equation (3.7) is then rewritten as

$$e^{j\phi} = \frac{1 - s_{33}^*\Gamma_N}{1 - s_{33}\Gamma_N} \quad . \tag{3.9}$$

If s_{33} is expressed as $s_{33} = a + jb$, equation (3.9) becomes

$$e^{j\phi} = \frac{1 + j\left(\frac{b\Gamma_N}{1 - a\Gamma_N}\right)}{1 - j\left(\frac{b\Gamma_N}{1 - a\Gamma_N}\right)} \quad , \tag{3.10}$$

where the function $\frac{b\Gamma_N}{1 - a\Gamma_N}$ is real. Since the form of Γ_N is arbitrary from a modeling viewpoint, the constants a and b may be equated to zero and one, respectively, such that

$$\boxed{s_{33} = j} \quad . \tag{3.11}$$

The choice to make s_{33} imaginary is considered suitable for the model of a microwave BJT, for example, where the nonlinear base-emitter junction is expected to be capacitive. In other applications, another choice for s_{33} may be appropriate.

3.3.3 Finding S_{13}/S_{23}

Expressions for model nodes b_1 and b_2 are written as

$$b_1 = s_{11}a_1 + s_{12}a_2 + s_{13}a_3 \tag{3.12}$$

$$b_2 = s_{21}a_1 + s_{22}a_2 + s_{23}a_3 \quad . \tag{3.13}$$

Equations (3.12) and (3.13) may be rearranged to solve for s_{13} and s_{23}, respectively, and the first result divided by the second to give

$$\frac{s_{13}}{s_{23}} = \frac{b_1 - s_{11}a_1 - s_{12}a_2}{b_2 - s_{21}a_1 - s_{22}a_2} \quad . \tag{3.14}$$

The numerator and denominator of the right side of (3.14) may be divided by a_1 to find the ratio of nonlinear parameters in terms of measured and known quantities as

$$r \equiv \frac{s_{13}}{s_{23}} = \frac{\Gamma - s_{11} - s_{12}\tau\Gamma_L}{\tau - s_{21} - s_{22}\tau\Gamma_L} \quad . \tag{3.15}$$

The ratio r in (3.15) is determined by utilizing the known small-signal parameters along with values of Γ and τ measured using either Γ_{L_1} or Γ_{L_2} at a high drive level such that Γ_N is non-zero.

3.3.4 Determining $S_{23}S_{31}$ and $S_{23}S_{32}$

It is desirable to isolate the remaining unknown parameters for solution. To do this, an expression is found for the large-signal model transmission for any given load reflection. First, the small-signal transmission, τ_0, is written from the model flow-graph as

$$\tau_0 = \frac{s_{21}}{1 - s_{22}\Gamma_L} \quad . \tag{3.16}$$

Next, (3.16) is subtracted from the general expression for transmission in (3.2) to give

$$\tau - \tau_0 = \frac{\left[\frac{s_{23}s_{31}}{1 - s_{22}\Gamma_L} + \frac{s_{23}s_{32}s_{21}\Gamma_L}{(1 - s_{22}\Gamma_L)^2}\right]\Gamma_N}{1 - \left[s_{33} + \frac{s_{23}s_{32}\Gamma_L}{1 - s_{22}\Gamma_L}\right]\Gamma_N} \quad . \tag{3.17}$$

Equation (3.17) has the form

$$\tau - \tau_0 = \frac{a\Gamma_N}{1 - b\Gamma_N} \quad , \tag{3.18}$$

where

$$a \equiv \frac{s_{23}s_{31}}{1 - s_{22}\Gamma_L} + \frac{s_{23}s_{32}s_{21}\Gamma_L}{(1 - s_{22}\Gamma_L)^2} \tag{3.19}$$

and

$$b \equiv s_{33} + \frac{s_{23}s_{32}\Gamma_L}{1 - s_{22}\Gamma_L} \quad . \tag{3.20}$$

The right sides of (3.18) and (3.5) are equated and rearranged to give

$$C_\tau e^{j\phi} = C_\tau - \frac{a\Gamma_N}{1 - b\Gamma_N}$$

$$= \frac{C_\tau - (a + bC_\tau)\Gamma_N}{1 - b\Gamma_N}$$

or

$$e^{j\phi} = \frac{1 - \left[\frac{a + bC_\tau}{C_\tau}\right]\Gamma_N}{1 - b\Gamma_N} \quad . \tag{3.21}$$

As in (3.7), the coefficients of Γ_N in (3.21) must be complex conjugates in order for the right side to have a magnitude of unity. Thus,

$$\frac{a + bC_\tau}{C_\tau} = b^*$$

or

$$a = C_\tau(b^* - b)$$

$$= -j2C_\tau\, Im(b) \quad . \tag{3.22}$$

The variables a and b in (3.22) may be replaced by (3.19) and (3.20), respectively, to give

$$\frac{s_{23}s_{31}}{1 - s_{22}\Gamma_L} + \frac{s_{23}s_{32}s_{21}\Gamma_L}{(1 - s_{22}\Gamma_L)^2} = -j2C_\tau\, Im\left(s_{33} + \frac{s_{23}s_{32}\Gamma_L}{1 - s_{22}\Gamma_L}\right) \quad . \tag{3.23}$$

The unknown quantities in (3.23) are $s_{23}s_{31}$ and $s_{23}s_{32}$. By using the two distinct values of load reflection, Γ_{L1} and Γ_{L2}, four equations are created that contain the real and imaginary components of the unknowns. Let subscript i, $i \in \{1,2\}$, designate correspondence to a particular load reflection and let

$$\alpha \equiv s_{23}s_{31} \tag{3.24}$$

$$\beta_i \equiv 1 - s_{22}\Gamma_{Li} \tag{3.25}$$

$$\gamma \equiv s_{23}s_{32} \ . \tag{3.26}$$

Thus, (3.23) becomes

$$\frac{\alpha}{\beta_i} + \frac{s_{21}\Gamma_{Li}\gamma}{\beta_i^2} = -j2C_{\tau_i} Im\left(s_{33} + \frac{\Gamma_{Li}\gamma}{\beta_i}\right)$$

or

$$\alpha + \frac{s_{21}\Gamma_{Li}\gamma}{\beta_i} = C_{\tau_i}\left[-\Gamma_{Li}\gamma - s_{33}\beta_i + \left(\frac{\Gamma_{Li}\gamma}{\beta_i}\right)^* \beta_i + s_{33}^*\beta_i\right] \ . \tag{3.27}$$

Rearranging (3.27) and making use of (3.11) gives the form

$$\alpha + a_i\gamma + b_i\gamma^* + c_i = 0 \ , \tag{3.28}$$

where

$$a_i \equiv \frac{s_{21}\Gamma_{Li}}{\beta_i} + C_{\tau_i}\Gamma_{Li}$$

$$b_i \equiv -\frac{C_{\tau_i}\beta_i\Gamma_{Li}^*}{\beta_i^*}$$

$$c_i \equiv j2\beta_i C_{\tau_i} \ .$$

To solve for γ, (3.28) is written for each load reflection and the resulting two equations are combined to eliminate α. The new equation, containing the unknowns γ and γ^*, is then decomposed into two real, independent equations

which can be solved simultaneously for the real and imaginary parts of γ. Solving for γ gives, after some simplification,

$$\gamma \equiv s_{23}s_{32} = \frac{A^*C - BC^*}{|B|^2 - |A|^2} \quad , \tag{3.29}$$

where

$$A \equiv a_1 - a_2$$

$$B \equiv b_1 - b_2$$

$$C \equiv c_1 - c_2 \quad .$$

With γ known, α is found from (3.28) as

$$\alpha \equiv s_{23}s_{31} = -(a_i\gamma + b_i\gamma^* + c_i) \quad , \tag{3.30}$$

with i equated to 1 or 2.

3.3.5 Solving For Individual Parameters

The large-signal parameters can be normalized to s_{31}, the drive to the nonlinear element from port 1. Thus, s_{31} is set to unity:

$$\boxed{s_{31} \equiv 1} \quad . \tag{3.31}$$

Then, from (3.30) and (3.31)

$$\boxed{s_{23} = \alpha} \tag{3.32}$$

and, from (3.15) and (3.32)

$$\boxed{s_{13} = s_{23}r} \quad . \tag{3.33}$$

Finally, s_{32} is found from (3.29) as

$$\boxed{s_{32} = \frac{\gamma}{s_{23}}} \quad . \tag{3.34}$$

3.3.6 Characterizing Γ_N

The last step in determining the model parameters is characterizing the value of the nonlinear element, Γ_N, versus drive level. From (3.18), Γ_N is expressed in terms of the measured transmission, τ, and the known model parameters as

$$\boxed{\Gamma_N = \frac{\tau - \tau_0}{a + b(\tau - \tau_0)}} \quad , \tag{3.35}$$

where a, b, and τ_0 are given by (3.19), (3.20), and (3.16), respectively. Using (3.35), a value for Γ_N is computed for each measured value of τ which, in turn, corresponds to a measured drive level at the model flow-graph input a_1. However, there is also the load-dependent contribution of input a_2 (via s_{32}) to the level at the input of the nonlinear element. Therefore, there is not a unique value of Γ_N for a given level at a_1 if the load reflection is not fixed. In order to be able to predict the value of Γ_N versus the a_1 level for any Γ_L, the relationship of the drive level at Γ_N, hereafter called a_N, to the level at a_1 must be known. From the model flow-graph and (3.31), a_N is found as

$$a_N = \frac{a_1 + s_{32}\Gamma_L \tau a_1}{1 - s_{33}\Gamma_N} \quad . \tag{3.35}$$

In general, only the magnitudes of the drive levels are of interest. Thus, (3.35) becomes

$$|a_N| = \left| \frac{a_1 + s_{32}\Gamma_L \tau a_1}{1 - s_{33}\Gamma_N} \right| \quad . \tag{3.36}$$

3.4 SUMMARY

In the familiar small-signal flow-graph characterization, a single drive level and a single termination—a load—are the requirements to find parameters which will enable prediction for any source and load terminations. Effectively then, it appears that in the characterization of the proposed nonlinear model, a minimum of additional measurements—made now over a range of drive levels and with two distinct terminations—allows the prediction of nonlinear behavior for any combination of a_1 and a_2 and thus by implication, any source and load terminations.

Chapter 4

Applications

4.1 INTRODUCTION

A model that is able to describe the nonlinear behavior of an active device lends itself to a variety of applications. For example, a nonlinear model could be used to predict the input reflection and output power level of a large-signal amplifier, for a given input power level and load impedance. The design of an oscillator might proceed by choosing a certain gain compression and output level as design constraints for a given load. A nonlinear model for the active device could then be utilized to predict the input reflection and transmission in order to design the oscillator feedback network.

To illustrate the applicability and verify the accuracy of the nonlinear model described in Chapter 3, this chapter will present three examples of its use. First, the model will be used to predict the input reflection and transmission of a typical microstrip amplifier, and these predictions will be compared with actual laboratory measurements. Second, the subject of stability in the context of large-signal amplifiers will be briefly addressed. Finally, the nonlinear model will be used to develop a new approach to oscillator design; this approach will be illustrated by converting the microstrip amplifier into an oscillator and showing through measurements that it meets the design goals.

4.2 PREDICTION OF INPUT REFLECTION AND TRANSMISSION

The nonlinear model in Fig. 3.1 can be utilized to predict the input reflection, Γ, and transmission, τ, of a modeled device. The device-under-test (DUT) must be first characterized using the method detailed in Section 3.3, which requires two arbitrary, distinct load terminations. In order to retain the applicability of the nonlinear model, care must be taken to avoid saturation of the DUT during the characterization and subsequent measurements.

The characterization of the DUT provides values for the linear portion of the model as well as tabular information about the nonlinear element, Γ_N. This tabular information provides the value of Γ_N versus the drive level a_N at port 3. A sample set of linear path values and a plot of associated values of Γ_N versus a_N are shown in Fig. 4.1. These data were derived from the characterization at 880 MHz of an MRF901 bipolar junction transistor (BJT) which was biased at 2 mA and connected as a common-emitter microwave amplifier. The characterization data were utilized in a comparison of model-predicted values of transmission and reflection with measured values. This device characterization was also used in an example of oscillator design.

To utilize the model for design, it is necessary to know the ratio of the magnitude of the input drive level, a_1, to the magnitude of the nonlinear element drive level, a_N, for a given load termination. From the model flow-graph (Fig. 3.1), the ratio of a_N to a_1 is found as

$$\frac{a_N}{a_1} = \frac{s_{31}(1 - s_{22}\Gamma_L) + s_{21}s_{32}\Gamma_L}{1 - s_{22}\Gamma_L - s_{33}\Gamma_N - (s_{23}s_{32} - s_{22}s_{33})\Gamma_N\Gamma_L} \quad . \tag{4.1}$$

s_{11}	.697 $\angle -149.03^\circ$
s_{12}	.138 $\angle 38.49^\circ$
s_{21}	2.315 $\angle 100.01^\circ$
s_{22}	.580 $\angle -.71^\circ$
s_{13}	3.232 $\angle -51.33^\circ$
s_{23}	7.287 $\angle -90.75^\circ$
s_{31}	1.00 $\angle 0^\circ$
s_{32}	.209 $\angle 76.02^\circ$
s_{33}	1.00 $\angle 90^\circ$

(a)

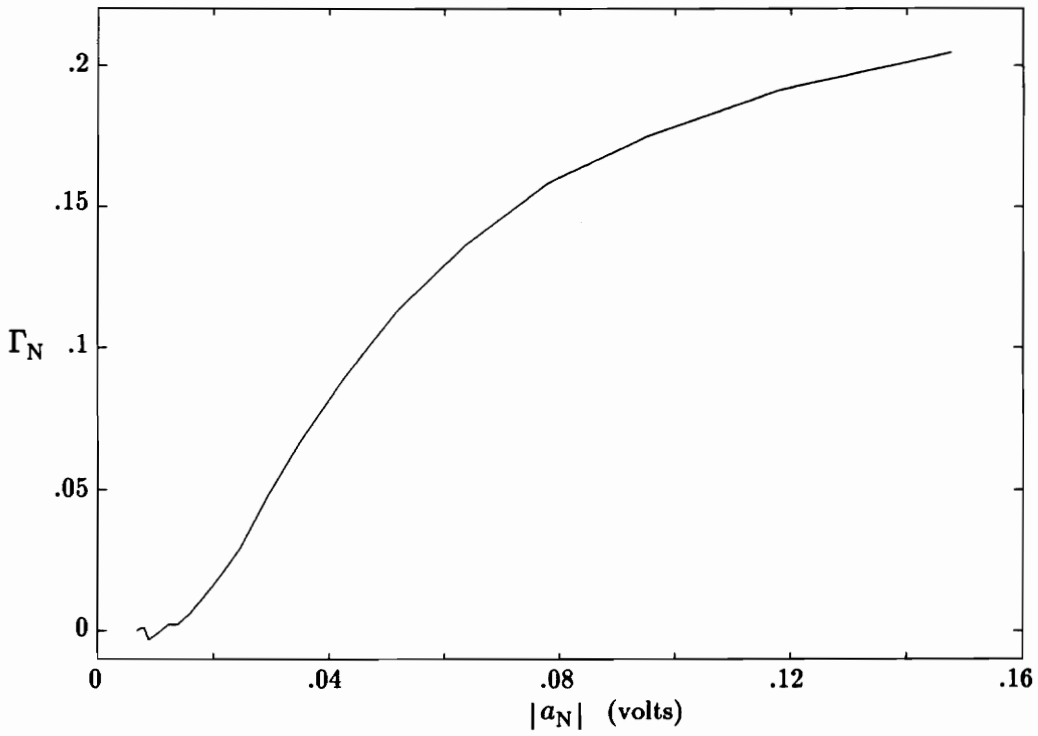

(b)

Figure 4.1. MRF901 BJT microwave amplifier characterization at 880 MHz, $I_c = 2$ mA. Values for the (a) linear and (b) nonlinear components in the nonlinear model shown in Fig. 3.1.

Then, from (4.1), the desired magnitude of a_1 is found as

$$|a_1| = \left| a_N \left[\frac{1 - s_{22}\Gamma_L - s_{33}\Gamma_N - (s_{23}s_{32} - s_{22}s_{33})\Gamma_N\Gamma_L}{s_{31}(1 - s_{22}\Gamma_L) + s_{21}s_{32}\Gamma_L} \right] \right| . \tag{4.2}$$

The formulas for input reflection and transmission given in Section 3.2 are

$$\Gamma = s_{11} + \frac{s_{13}s_{31}\Gamma_N(1 - s_{22}\Gamma_L) + s_{21}s_{12}\Gamma_L(1 - s_{33}\Gamma_N) + s_{31}s_{23}s_{12}\Gamma_N\Gamma_L}{1 - s_{22}\Gamma_L - s_{33}\Gamma_N - (s_{23}s_{32} - s_{22}s_{33})\Gamma_N\Gamma_L} , \tag{3.1}$$

$$\tau = \frac{s_{21}(1 - s_{33}\Gamma_N) + s_{31}s_{23}\Gamma_N}{1 - s_{22}\Gamma_L - s_{33}\Gamma_N - (s_{23}s_{32} - s_{22}s_{33})\Gamma_N\Gamma_L} . \tag{3.2}$$

The known model parameters—both the linear components and the tabular data of Γ_N versus a_N—are substituted in (3.1), (3.2), and (4.2) to obtain, in tabular form, predicted values of Γ and τ versus $|a_1|$. For a valid comparison between measured data and model-predicted values of Γ and τ, the load termination, Γ_L, that is employed here must be distinct from the two terminations used for the model characterization. This requirement assures mathematical independence between the computation of the model parameters and the computation of predicted Γ and τ. The three terminations employed for this work were an open, short, and load.

Measured data and model-predicted values of transmission and reflection are shown in Figs. 4.2 and 4.3 for the microstrip amplifier of Fig. 4.1. The accuracy of the magnitude and phase predictions for transmission is excellent. The constant one-degree phase error may be the result of a repeatability problem. The accuracy of the reflection magnitude prediction is also quite good, while the worst-case error in the reflection phase prediction is seven degrees. Closer agreement is expected for the case of transmission because the model development was based on a circle-

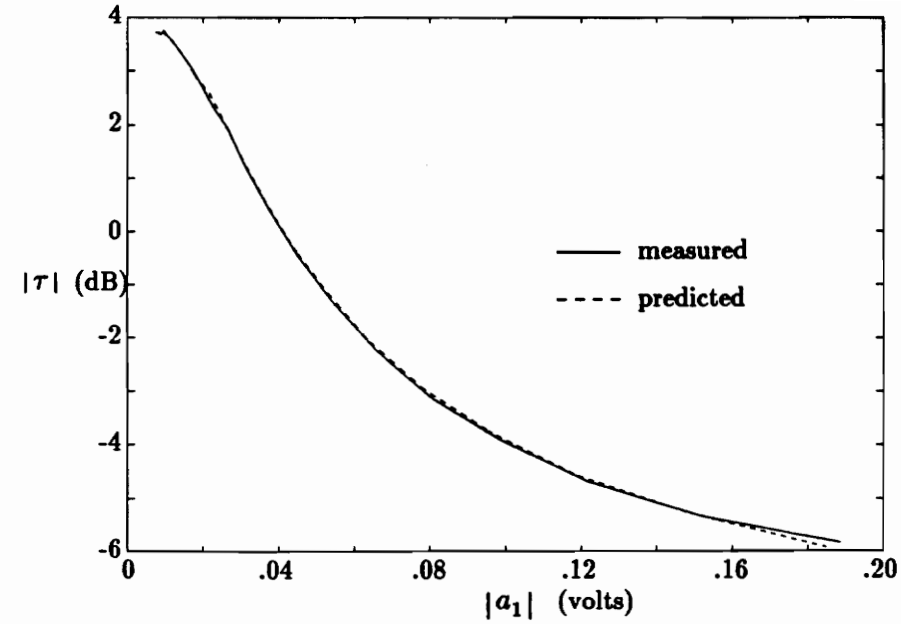

(a)

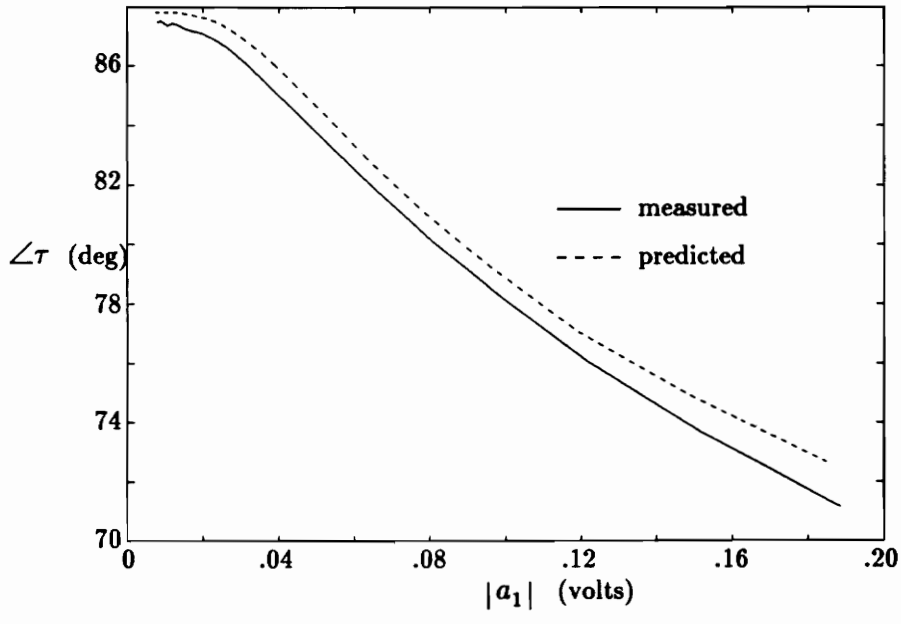

(b)

Figure 4.2. Measured and predicted transmission (a) magnitude and (b) phase versus input drive level for MRF901 BJT microwave amplifier.

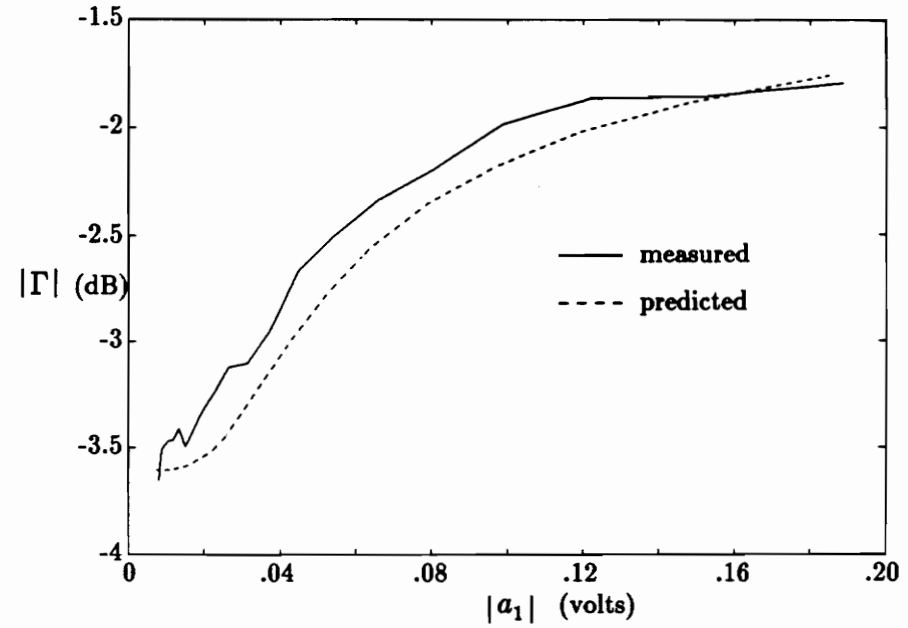

(a)

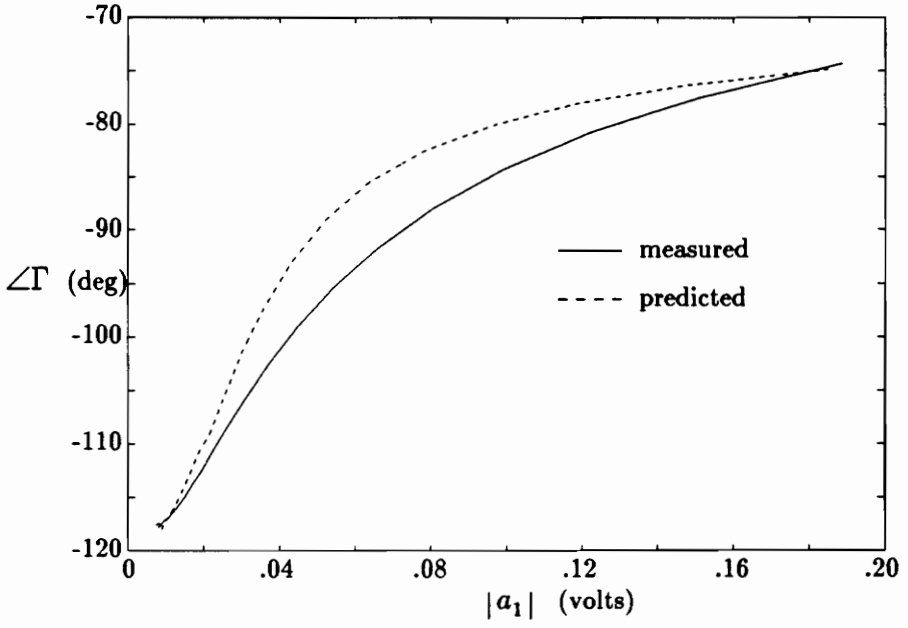

(b)

Figure 4.3. Measured and predicted reflection (a) magnitude and (b) phase versus input drive level for MRF901 BJT microwave amplifier.

fitting to transmission data. Overall, the results are reasonable for predictions based on measured data. Potential nonlinearities of the measurement system have been neglected, possibly explaining the deviation in the reflection results.

4.3 STABILITY

If a nonlinear model is to be utilized in the design of an amplifier, the large-signal stability of the amplifier should be considered. As a nonlinear model would most likely be used in the design of large-signal devices such as power amplifiers, it is appropriate to consider extending the familiar small-signal stability criteria to large-signal operation.

The small-signal stability of an amplifier may be determined by applying the well-known stability criteria [Carson, 1975] to the S parameters of the active device and the reflection coefficients of the terminations. This approach to stability analysis may be extended to a large-signal amplifier *for a given input drive level.* The equivalent two-port S parameters that describe the amplifier at the given drive level are used as in the small-signal case. These so-called large-signal S parameters may be measured [Leighton *et al*, 1973], or computed from the nonlinear model of Chapter 3. From Fig. 3.1, the large-signal S parameters, denoted here as s'_{ij}, $i,j \in \{1,2\}$, are given as

$$s'_{ij} = s_{ij} + \frac{s_{i3}s_{3j}\Gamma_N}{1 - s_{33}\Gamma_N} \quad , \tag{4.3}$$

where the value of Γ_N corresponds to the given drive level.

A stability analysis of a linear system may be expanded to include the notion of relative stability, the effect of a perturbation on the nominal stable

operating condition. The relative stability of a large-signal amplifier might be determined by the use of a set of incremental S parameters which describe the behavior of small-signal variations on a nominal large-signal excitation. For illustration, an expression for s_{11} in an incremental sense, $s_{11}^{\Delta} \equiv \frac{\partial b_1}{\partial a_1}$, will be found, again from Fig. 3.1. The output b_1 may be written in terms of the inputs a_1 and a_2 as

$$b_1 = \left(s_{11} + \frac{s_{13}s_{31}\Gamma_N}{1 - s_{33}\Gamma_N} \right) a_1 + \left(s_{12} + \frac{s_{13}s_{32}\Gamma_N}{1 - s_{33}\Gamma_N} \right) a_2 \quad . \tag{4.4}$$

Equation (4.4) may be differentiated with respect to a_1 to give

$$s_{11}^{\Delta} = s_{11} + \frac{s_{13}s_{31}\Gamma_N}{1 - s_{33}\Gamma_N} + \left[\frac{s_{13}s_{31}a_1 + s_{13}s_{32}a_2}{(1 - s_{33}\Gamma_N)^2} \right] \frac{\partial \Gamma_N}{\partial a_1} \quad . \tag{4.5}$$

If the partial derivative $\frac{\partial \Gamma_N}{\partial a_1}$ in (4.5) is set to zero, the incremental S parameter s_{11}^{Δ} reverts to the large-signal form of (4.3). It must be noted that this partial derivative does not, strictly speaking, exist because its value is dependent on the phase of the small-signal perturbation relative to the large-signal excitation. This problem may be resolved by decomposing the partial derivative into in-phase and quadrature components and computing the incremental S parameters for each case. The resulting two sets of S parameters should be used, in turn, in the determination of network stability.

Incremental S parameters might also be applied to an amplitude stability analysis of an oscillator, offering the potential of predicting oscillator squegging (or motorboating). Further work in the area of stability is recommended.

4.4 OSCILLATOR DESIGN

There are three fundamental components of a sinewave oscillator—an amplifier or active device, a feedback network, and an output load. Noise that is present at the instant when power is applied to the oscillator is amplified, filtered and reapplied to the amplifier input. If the amplifying device and feedback network are described with the usual small-signal models, it is expected from analysis that the amplifier output will increase without bound—an impossible scenario. The physical mechanism that provides amplitude stabilization is usually the nonlinear behavior of the amplifier, that is, the amplifier gain decreasing as the signal at its input grows. Thus, an amplifier used in this application is a candidate for the nonlinear model described in the previous chapter.

4.4.1 Choosing Value for Γ_N

The first step in the design of an oscillator using the nonlinear model in Fig. 3.1 is to plot the values of the nonlinear element, Γ_N, versus the port 3 drive level, called a_N, that were obtained in tabular form from the model characterization. The plot of Γ_N that represents the particular device used for this example is shown in Fig. 4.1. Operating characteristics of the oscillator are determined by selecting a value for Γ_N. To enhance the oscillator amplitude stability, a desirable choice for Γ_N would be in the region where Γ_N exhibits the greatest change with respect to drive level. Within this region, a higher operating level may tend to accentuate harmonic production, while too low a level may cause unreliable startup. Once the choice of Γ_N has been made, the three-port nonlinear model may be reduced to a two-port equivalent with the resulting flow-graph paths designated by primed quantities. With the output load incorporated into the feedback network, an

oscillator may then be represented as the connection of two-port flow-graphs as shown in Fig. 4.4a.

4.4.2 Oscillator Topology

The design of the oscillator proceeds here with the assumption that the feedback existing within the active device itself is sufficient to support oscillation given certain source and load terminations, Γ_S and Γ_L. Thus, the transmission portion of the feedback network may be eliminated so that

$$s_{12}^F = s_{21}^F \equiv 0 \quad . \tag{4.6}$$

The representation of an oscillator having the constraint of (4.6) is shown in Fig. 4.4b.

4.4.3 Finding Source and Load Terminations

The reflection coefficient looking into port 2 of the active device is given by

$$\Gamma_2 = s'_{22} + \frac{s'_{12}s'_{21}\Gamma_S}{1 - s'_{11}\Gamma_S} \quad . \tag{4.7}$$

A necessary condition for oscillation is that terminations, Γ_S and Γ_L, must be connected to port 1 and port 2 such that

$$\Gamma_2\Gamma_L \equiv 1 \quad . \tag{4.8}$$

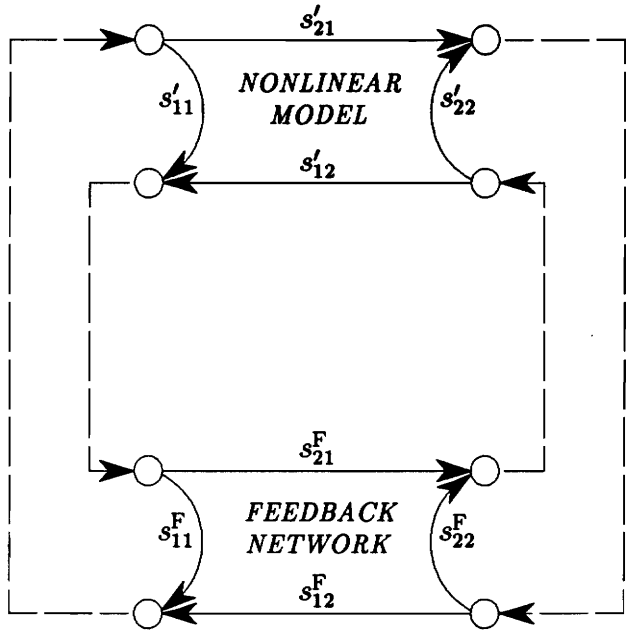

(a)

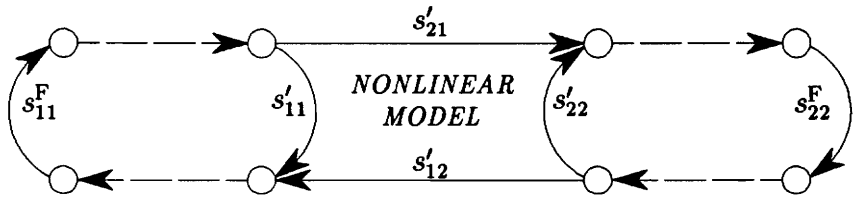

(b)

Figure 4.4. (a) Generalized representation of an oscillator as the connection of a nonlinear active device model with a feedback network. (b) Representation of oscillator topology chosen for design: $s^{F}_{12} = s^{F}_{21} \equiv 0$.

Similarly, Γ_1, the reflection coefficient looking into port 1 of the active device, may be expressed in terms of Γ_L; a second necessary condition for oscillation is that

$$\Gamma_1\Gamma_S \equiv 1 \quad . \tag{4.9}$$

Equations (4.8) and (4.9) imply that the active device is potentially unstable and that the condition of resonance exists at ports 1 and 2. It may be shown [Gonzalez, 1984] that if (4.8) is satisfied, (4.9) must be satisfied, and vice versa.

From (4.7) and (4.8),

$$\Gamma_L = \frac{1 - s'_{11}\Gamma_S}{s'_{22} - \Delta_S\Gamma_S} \quad , \tag{4.10}$$

where

$$\Delta_S \equiv s'_{11}s'_{22} - s'_{12}s'_{21} \quad .$$

The source termination, $\Gamma_S \equiv s^F_{11}$, may be considered as one side of a pi-network, a common feedback topology for oscillators. The internal feedback of the active device, s'_{12}, would serve as the middle element—likely being capacitive—and the load termination, $\Gamma_L \equiv s^F_{22}$, would represent the other side. Thus, Γ_S may be constrained to be purely reactive, that is,

$$|\Gamma_S| \equiv 1 \quad . \tag{4.11}$$

The constraint of (4.11) implies that Γ_S will have the locus of a circle with center at zero and radius of one given by

$$\Gamma_S = e^{j\theta} \quad . \tag{4.12}$$

The expression for Γ_L in (4.10) is a bilinear transformation of the variable Γ_S. Because Γ_S is constrained to have the locus of a circle, the quantity Γ_L also has the locus of a circle. It may be shown (see Appendix) that, given a known bilinear transformation of a variable having the locus of a known circle, the center and radius of the transformed circle may be found. For the bilinear transformation of Γ_S, the resulting center and radius of the Γ_L circle may be determined, respectively, as

$$C_L = \frac{(s'_{22})^* - s'_{11}\Delta_S^*}{|s'_{22}|^2 - |\Delta_S|^2} \tag{4.13}$$

and

$$R_L = \left| \frac{s'_{12}s'_{21}}{|s'_{22}|^2 - |\Delta_S|^2} \right| . \tag{4.14}$$

The load reflection circle may be plotted using (4.13) and (4.14). The output load to which power must be delivered is incorporated in Γ_L. Therefore, Γ_L must be passive given by

$$|\Gamma_L| < 1 .$$

A passive load reflection exists if

$$\big||C_L| - R_L\big| < 1 , \tag{4.15}$$

that is, if at least some portion of the load reflection circle lies in the region in the reflection plane representing $|\Gamma| < 1$. If (4.15) does not hold, the above procedure may be repeated after choosing another value for Γ_N, shifting the DC bias point of the active device, or selecting another active device type. Once (4.15) has been satisfied, a specific point on the Γ_L circle may be selected based on considerations

such as ease of design or construction. In the example that follows, the point closest to the origin was selected to keep the transformation ratio in the output matching network as close to unity as possible. In this case, Γ_L is given by

$$\Gamma_L = C_L - R_L e^{j\angle C_L} \quad . \tag{4.16}$$

With Γ_L known, Γ_S may be determined from a rearrangement of (4.10):

$$\Gamma_S = \frac{1 - s'_{22}\Gamma_L}{s'_{11} - \Delta_S \Gamma_L} \quad . \tag{4.17}$$

After Γ_S is determined from (4.17), a check on the result may be made by verifying (4.11).

Because, in practice, a lossless source termination is impossible to implement, the required load termination will differ somewhat from the originally selected value. Therefore, the magnitude of Γ_S should be reduced by a factor based on a loss estimate or a direct measurement of the source termination. The final value of Γ_L may then be computed from (4.10).

4.4.4 Output Level Prediction

After the source and load terminations have been computed, the output level of the designed oscillator may be predicted. The level at node a_3 in Fig. 3.1 is given by

$$a_3 = a_N \Gamma_N \quad , \tag{4.18}$$

where Γ_N is the value chosen in the design procedure for the nonlinear reflection coefficient and a_N is the corresponding drive level at port 3. The value of a_N may be found by interpolating the tabular information of Γ_N versus a_N that was produced as part of the nonlinear model characterization.

The ratio of b_2 to a_3 in Fig. 3.1 is computed as

$$\frac{b_2}{a_3} = \frac{s_{23}(1 - s_{11}\Gamma_S) + s_{13}s_{21}\Gamma_S}{1 - s_{11}\Gamma_S - s_{22}\Gamma_L + \Delta_S\Gamma_S\Gamma_L} \quad , \tag{4.19}$$

where Γ_S and Γ_L are the design source and load terminations, respectively, and

$$\Delta_S \equiv s_{11}s_{22} - s_{21}s_{12} \quad .$$

In the measurement system shown in Fig. 2.3, the oscillator power delivered to Γ_L may be measured at node b_2'. The predicted output power level at b_2' is given by

$$b_2'\big|_{\text{dBm}} = 10\log\left[\frac{|b_2|^2(1 - |\Gamma_L|^2)|A|^2|e_{32}|^2}{.05}\right] \quad , \tag{4.20}$$

where the factor $(1 - |\Gamma_L|^2)$ accounts for the inclusion of a matching network cascaded to the b_2-a_2 nodes in the figure. The factor b_2 may be found from (4.18) and (4.19). The factors A and e_{32} are measurement system quantities discussed in Section 2.4. Equation (4.20) assumes a lossless output matching network and a 50Ω reference impedance.

4.4.5 Results

Common-emitter measurements of an MRF901 BJT microwave amplifier were made at 880 MHz for the characterization of the nonlinear model introduced in Chapter 3. The resulting characterization data were presented in Fig. 4.1. An oscillator was subsequently designed using the above procedure and constructed with microstrip techniques. The oscillator layout is shown in Fig. 4.5.

As an intermediate step in the design procedure, the reflection at the transistor input was both measured and predicted with the design value of Γ_L connected at the output. The results are shown in Fig. 4.6. The magnitude of the input reflection is seen to be greater than unity over a range of input drive levels—the expected condition for a potential oscillator.

The computed source reflection termination was then connected at the transistor input and oscillation was observed on a spectrum analyzer connected to port b_2'. The measured oscillator frequency was 900 MHz and the measured output level was −31.5 dBm. The power actually delivered to Γ_L would be approximately 20 dB greater, after accounting for the Ae_{32} isolation factor for port b_2'.

The measured output level was about 1.5 dB lower than the predicted value. This small discrepancy may be accounted for by the slight error observed in the input reflection magnitude prediction shown in Fig. 4.6a and by loss in the output matching network.

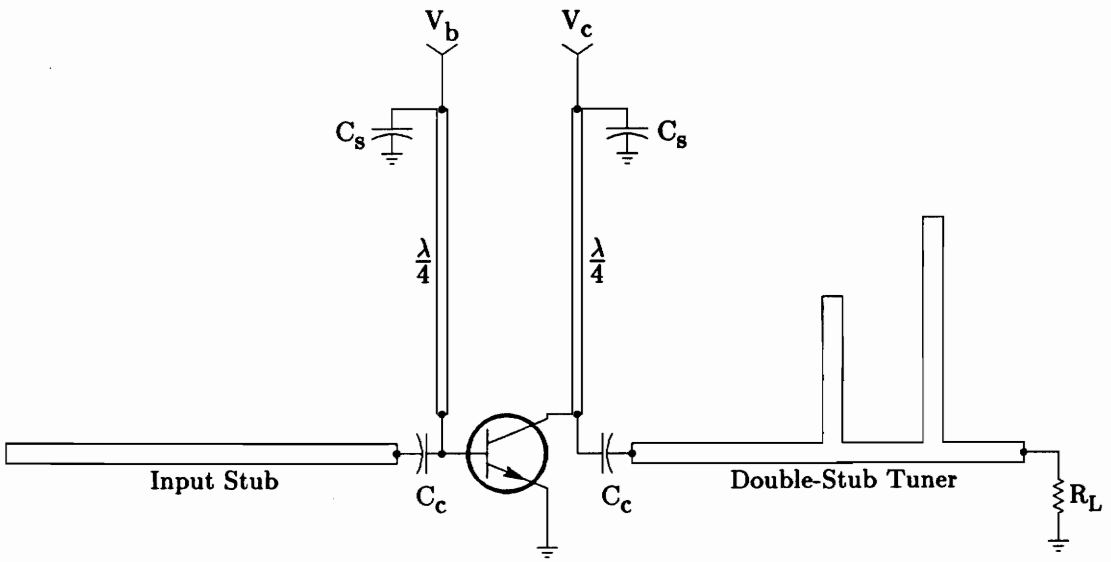

Figure 4.5. Microstrip 880 MHz oscillator. Coupling capacitors and bias networks were used during the transistor characterization; to construct an oscillator, the two output tuning stubs were added and the input line was cut to form the input stub. Bypass capacitors, C_S, were constructed using microstrip patches; coupling capacitors, C_C, were 100 pF chips. Bias voltages, V_b and V_C, were derived from a collector-feedback resistor network. Load resistor, R_L, was a 50Ω termination.

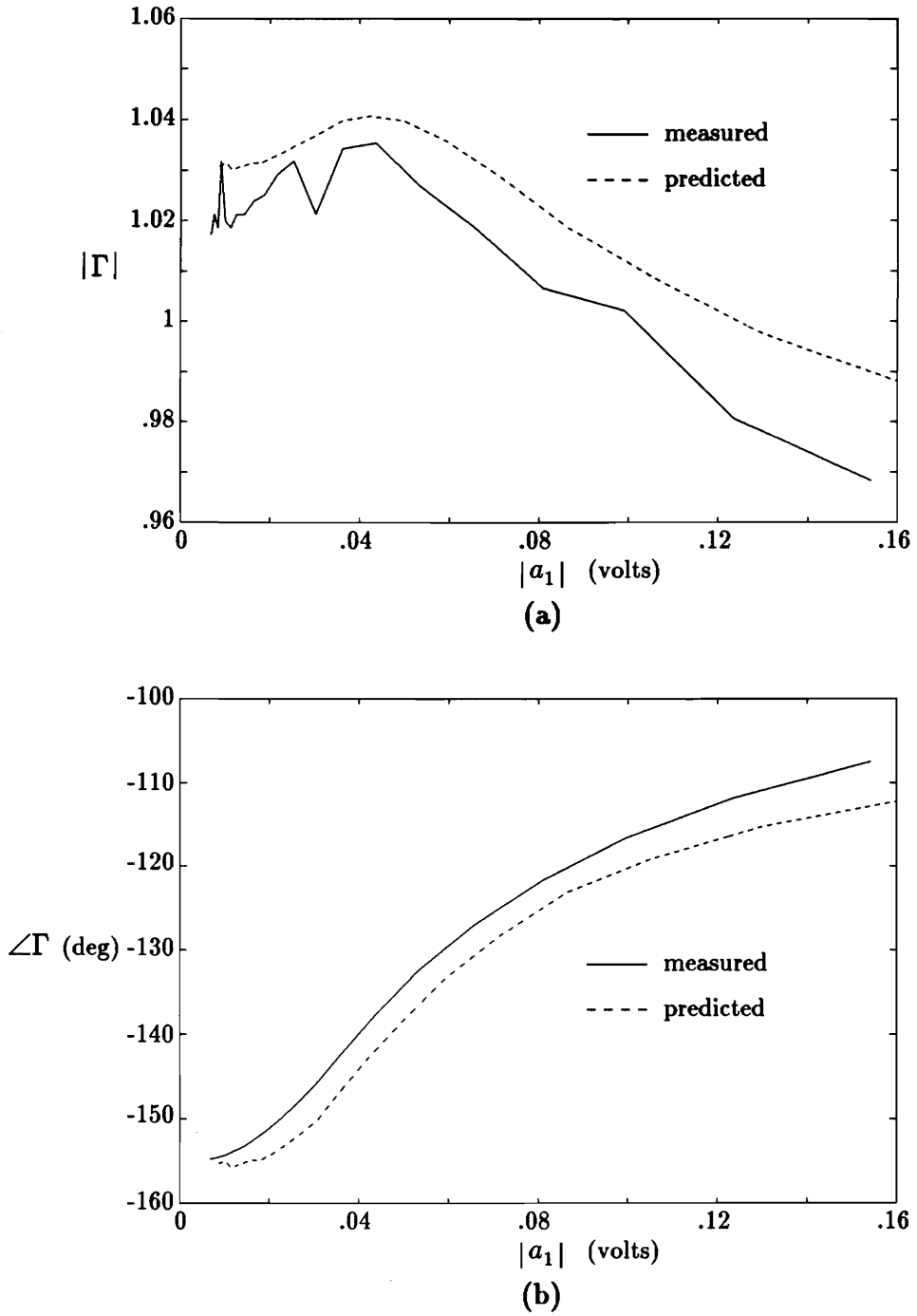

Figure 4.6. Measured and predicted input reflection coefficient (a) magnitude and (b) phase versus input drive level for MRF901 BJT microwave amplifier with load reflection chosen for instability.

Chapter 5

Conclusion

Current approaches to the analysis of nonlinear devices at microwave frequencies generally rely on complex, physically-based models that require powerful computational tools for their use. Previous attempts at developing parameter-based models have resulted in descriptions that are termination-specific or that have questionable validity in a nonlinear environment. This thesis has provided a simple S-parameter-based model that may be used to accurately predict—for arbitrary source or load terminations—the nonlinear behavior of a two-port device exhibiting a single nonlinearity.

The nonlinear model was shown to be realizable with a conventional 3-port flow-graph having a real-valued, nonlinear reflection terminating one of the ports. A procedure was developed for computing the model parameters from measured values of device transmission and reflection. The ability of the characterized nonlinear model to predict device performance for an arbitrary load termination was verified by comparisons of measured and predicted data for both device transmission and reflection.

The concepts of large-signal and incremental stability were discussed. It was shown that both types of stability could be determined by computing the so-called large-signal and incremental S parameters using the nonlinear model.

The design procedure for a microwave oscillator was given as an application of the nonlinear model. An oscillator was constructed using microstrip techniques and the measured results showed good agreement with the model predictions.

This thesis has also described a new one-way, two port measurement system that is suitable for the characterization of nonlinear devices. The system provides the necessary independent control of the incident voltages at the device ports without requiring source switching or device reversal. Calibrated measurements of device reflection and transmission for a chosen load reflection may be made using the system and such measurements were utilized for the nonlinear model characterization. In addition, it was shown that by making device measurements with two distinct terminations, the small-signal S parameters could be determined.

Adapting the nonlinear model for broadband device characterization is an avenue for future work. A more general stability formulation could be explored. In addition, it is suggested that the linearity and repeatability of the measurement system be examined.

REFERENCES

Barr, J.T. and M.J. Pervere (1989), "A Generalized Vector Network Analyzer Calibration Technique," *34th ARFTG Digest.*

Carson, R.S. (1975), *High Frequency Amplifiers.* John Wiley & Sons, New York.

Davis, W.A. (1991), Personal communication, VPI & SU.

Davis, W.A. and D.M. Keller (1991), Personal communication, VPI & SU.

Engen, G.F. and C.A. Hoer (1979), "An Improved Technique for Calibrating the Dual Six-Port Automatic Network Analyzer," *IEEE Trans. Microwave Theory Tech.*, Vol. MTT-27, No. 12, pp. 987-993.

Eul, H.J. and B. Schiek (1988), "Thru-Match-Reflect: One Result of a Rigorous Theory for De-Embedding and Network Analyzer Calibration," *Proc. 18th European Microwave Conf.*, pp. 909-914.

Gilmore, R.J. and F.J. Rosenbaum (1983), "An Analytic Approach to Optimum Oscillator Design Using S-Parameters," *IEEE Trans. Microwave Theory Tech.*, Vol. MTT-31, No. 8, pp. 633-639.

Gonzalez, G. (1984), *Microwave Transistor Amplifiers.* Prentice-Hall, Inc., Englewood Cliffs, New Jersey.

Hejhall, R. (1985), "Small-Signal Parameters Aid FET Power-Amp Design," *Microwaves & RF*, Vol. 24, No. 9, pp. 141-144.

Kasa, I. (1976), "A Circle-Fitting Procedure and its Error Analysis," *IEEE Transactions on Instrumentation and Measurement*, Vol. IM-25, No. 1, pp. 7-14.

Kasa, I. (1974), "Closed-Form Mathematical Solutions to Some Network Analyzer Calibration Equations," *IEEE Transactions on Instrumentation and*

Measurement, Vol. IM-23, No. 4, pp. 309-402.

Khramov, A.V. (1983), "Measurement of the S-Parameters of Transistors Under Large-Signal Conditions," *Telecommunications and Radio Engineering*, Vol. 38, pp. 123-124.

Leighton, W.H., R.J. Chaffin, and J.G. Webb (1973), "RF Amplifier Design with Large-Signal S-Parameters," *IEEE Trans. Microwave Theory Tech.*, Vol. MTT-21, No. 12, pp. 809-814.

Mokari-Bolhassan, M.E. and W.K. Wong (1989), "Design and Analysis of Large-Signal Microwave Power Amplifiers," *IEEE International Symposium on Circuits and Systems*, Vol. 3, pp. 2231-2234.

Peterson, D.L., A.M. Pavio, and B. Kim (1984), "A GaAs FET Model for Large-Signal Applications," *IEEE Trans. Microwave Theory Tech.*, Vol. MTT-32, No. 3, pp. 276-281.

Rytting, D. (1982), "An Analysis of Vector Measurement Accuracy Enhancement Techniques," (Hewlett Packard) Paper given at RF & Microwave Measurement Symposium and Exhibition, March.

Toropov, E.B. (1981), "Measurement of the S-Parameters of Transistors in the Large-Signal Mode," *Telecommunication and Radio Engineering*, Vol. 36, pp. 116-117.

Tucker, R.S. (1981), "RF Characterization of Microwave Power FET's," *IEEE Trans. Microwave Theory Tech.*, Vol. MTT-29, No. 8, pp. 776-781.

van der Puije, P.D. and S.R. Mazumder (1978), "Two-Signal Method of Measuring the Large-Signal S-Parameters of Transistors," *IEEE 1978 MTT-S International Microwave Symposium Digest*, pp. 263-265.

Vendelin, G.D., A.M. Pavio, and U.L. Rohde (1990), *Microwave Circuit Design Using Linear and Nonlinear Techniques*. John Wiley & Sons, New York.

Appendix

Bilinear Transformation of a Known Circle

It will be shown that, for a given bilinear transformation of a variable having the locus of a known circle, the center and radius of the transformed circle may be determined. Though the results may be found in the literature, the development presented here was prepared by Dr. William A. Davis of Virginia Polytechnic Institute.

The general form of a bilinear transformation is given as

$$w = \frac{a + bz}{c + dz} \quad , \tag{A.1}$$

where a through d are known constants and z is the independent variable. Let z have the locus of a circle such that

$$z = A + Be^{j\phi} \quad , \tag{A.2}$$

where A and B are, respectively, the known center and radius.

Equation (A.1) may be rewritten to give

$$w = \frac{\frac{b}{d}(c + dz) + (a - \frac{bc}{d})}{c + dz}$$

$$= \frac{b}{d} + \left(\frac{ad - bc}{d}\right)\frac{1}{c + dz} \quad . \tag{A.3}$$

Equation (A.2) may be substituted in (A.3) to give

$$w = \frac{b}{d} + \left(\frac{ad-bc}{d}\right)\frac{1}{(c+dA)+dBe^{j\phi}} \quad . \tag{A.4}$$

Finally, (A.4) may be multiplied and divided by the factor

$$\left[(c+dA)^* - dBe^{j\phi}\frac{(c+dA)^* + d^*B^*e^{-j\phi}}{(c+dA)+dBe^{j\phi}}\right] ,$$

to give

$$w = \frac{b}{d} + \left(\frac{ad-bc}{d}\right)\frac{\left[(c+dA)^* + dBe^{j\theta}\right]}{|c+dA|^2 - |dB|^2} \quad . \tag{A.5}$$

If equation (A.5) is rewritten in the form $w = C + Re^{j\alpha}$, where C and R are the center and radius of the transformed circle, respectively, then

$$C = \frac{b}{d} + \left(\frac{ad-bc}{d}\right)\frac{(c+dA)^*}{|c+dA|^2 - |dB|^2} \quad , \tag{A.6}$$

$$R = \frac{|ad-bc|B}{\left||c+dA|^2 - |dB|^2\right|} \quad . \tag{A.7}$$

Thus, circle z with center A and radius B is transformed by (A.1) to a new circle w with center C and radius R given by (A.6) and (A.7), respectively. It should be noted that the relationship between ϕ and α has not been established, that is, there is not a point-by-point correspondence between the original and transformed circles.

VITA

Marc William Legori Ditz was born to Gerhard William Ditz and Gloria Legori Ditz in New York City on May 22, 1957. He graduated from Charleston (Illinois) High School in 1975 and then spent three years completing the pre-engineering program at Eastern Illinois University. During this time he operated a small business within a retail storefront repairing high-fidelity audio equipment. He later transferred to the University of Illinois in Urbana and received a BSEE in 1980.

After graduation, he worked for two years at Tecnetics, Inc. in Boulder, Colorado as a design engineer in the area of switching power supplies. He was later employed for six years as a project engineer with Lifeline Systems, Inc. in Watertown, Massachusetts. There, he developed low-power RF (300 MHz) links for use in the company's personal emergency response products.

In 1990, he enrolled as a Masters student in the Electrical Engineering department at Virginia Polytechnic Institute and State University in Blacksburg. During the second year of his graduate studies he was awarded a tuition waiver and he received additional financial support in the form of corporate research funding and a graduate teaching assistantship. He received a Master of Science degree in the fall of 1992.

His current avocational interests include listening to classical and jazz music, reading, hiking, and bread baking.